

Sleep loss diminishes hippocampal reactivation and replay

<https://doi.org/10.1038/s41586-024-07538-2>

Received: 1 February 2023

Accepted: 7 May 2024

Published online: 12 June 2024

 Check for updates

Bapun Giri^{1,2,5}, Nathaniel Kinsky^{1,5}, Utku Kaya¹, Kourosh Maboudi^{1,2}, Ted Abel³ & Kamran Diba^{1,4}✉

Memories benefit from sleep¹, and the reactivation and replay of waking experiences during hippocampal sharp-wave ripples (SWRs) are considered to be crucial for this process². However, little is known about how these patterns are impacted by sleep loss. Here we recorded CA1 neuronal activity over 12 h in rats across maze exploration, sleep and sleep deprivation, followed by recovery sleep. We found that SWRs showed sustained or higher rates during sleep deprivation but with lower power and higher frequency ripples. Pyramidal cells exhibited sustained firing during sleep deprivation and reduced firing during sleep, yet their firing rates were comparable during SWRs regardless of sleep state. Despite the robust firing and abundance of SWRs during sleep deprivation, we found that the reactivation and replay of neuronal firing patterns was diminished during these periods and, in some cases, completely abolished compared to ad libitum sleep. Reactivation partially rebounded after recovery sleep but failed to reach the levels found in natural sleep. These results delineate the adverse consequences of sleep loss on hippocampal function at the network level and reveal a dissociation between the many SWRs elicited during sleep deprivation and the few reactivations and replays that occur during these events.

Memories undergo continuous refinement following learning, in a process referred to as memory consolidation in which sleep plays a critical role. Sleep immediately after learning benefits memories¹ and memories can be disrupted by even a few hours of sleep loss³. Studies have highlighted the importance of the hippocampus for sleep-dependent memory consolidation. However, the mechanisms through which memories are impacted by sleep loss have yet to be understood. Hippocampal sharp-wave ripples (SWRs), which feature sharp waves in the dendrites of CA1 pyramidal cells coupled with ripple oscillations (150–250 Hz) near the cell bodies, are widely considered to play a critical role in sleep-dependent memory processes. SWRs are observed more frequently in sleep after memory tasks⁴. Disrupting activity during these oscillations impairs memory^{5,6}, whereas enhancing them improves memory⁷.

A key characteristic of SWRs is that they are generated in the CA3 region of the hippocampus and then produce intense spiking activity throughout the hippocampal formation⁸ and beyond^{9–11}. Such synchronized activity drives synaptic plasticity in the network connections associated with individual memories, enhancing their storage and recall^{12,13}. In fact, both synaptic strengthening, by means of long-term potentiation^{14,15}, and synaptic weakening, through depotentiation or long-term depression^{16,17}, have been associated with SWRs. In particular, the spiking activity during SWRs can be highly patterned to reactivate and replay activities initially expressed during learning and behaviour in a temporally compressed manner akin to rapid rehearsal¹⁸. By generating such rehearsals, SWRs can strengthen and stabilize spatial

representations in the hippocampus^{6,19} and broadcast this signal to cortical and subcortical brain regions^{8,9}. Although reactivations and replays during SWRs are widely considered to play a key role in the memory consolidation process, nothing is known about how these events are impacted by sleep deprivation (SD).

Long-duration recordings during behaviour, sleep and sleep deprivation

We performed extracellular recordings using 128-channel high-density silicon probes implanted unilaterally and bilaterally in the CA1 region of the rat hippocampus (Methods) during behaviour and sleep. We tracked local field potentials (LFPs) and stable units putatively classified into 754 pyramidal neurons and 96 interneurons. Recordings were initiated approximately 3.5 h before the onset of the light cycle with about 2.5 h of rest and sleep in a home cage (PRE). Animals were then placed in linear maze environments of differing shapes (MAZE), which they had not previously explored, and were allowed to run for about 1 h for water reward. Following the maze, animals were returned to the home cage for POST sessions, which involved either natural (ad libitum) sleep and rest (non-sleep deprivation (NSD)) for 9 h or SD through gentle handling for 5 h followed by recovery sleep (RS) (Fig. 1a). We divided these periods into 2.5 h blocks (NS1–NS3 versus SD1–SD2 and RS) aligned to zeitgeber time = 0, the onset of the light cycle. We then compared RS to NS1, the first blocks of ad libitum sleep in each group, as well as SD2 versus NS2, to show the effects of prolonged wakefulness

¹Department of Anesthesiology, University of Michigan Medical School, Ann Arbor, MI, USA. ²Department of Psychology, University of Wisconsin-Milwaukee, Milwaukee, WI, USA. ³Department of Neuroscience and Pharmacology, Iowa Neuroscience Institute, University of Iowa, Iowa City, IA, USA. ⁴Neuroscience Graduate Program, University of Michigan, Ann Arbor, MI, USA. ⁵These authors contributed equally: Bapun Giri, Nathaniel Kinsky. ✉e-mail: kdiba@umich.edu

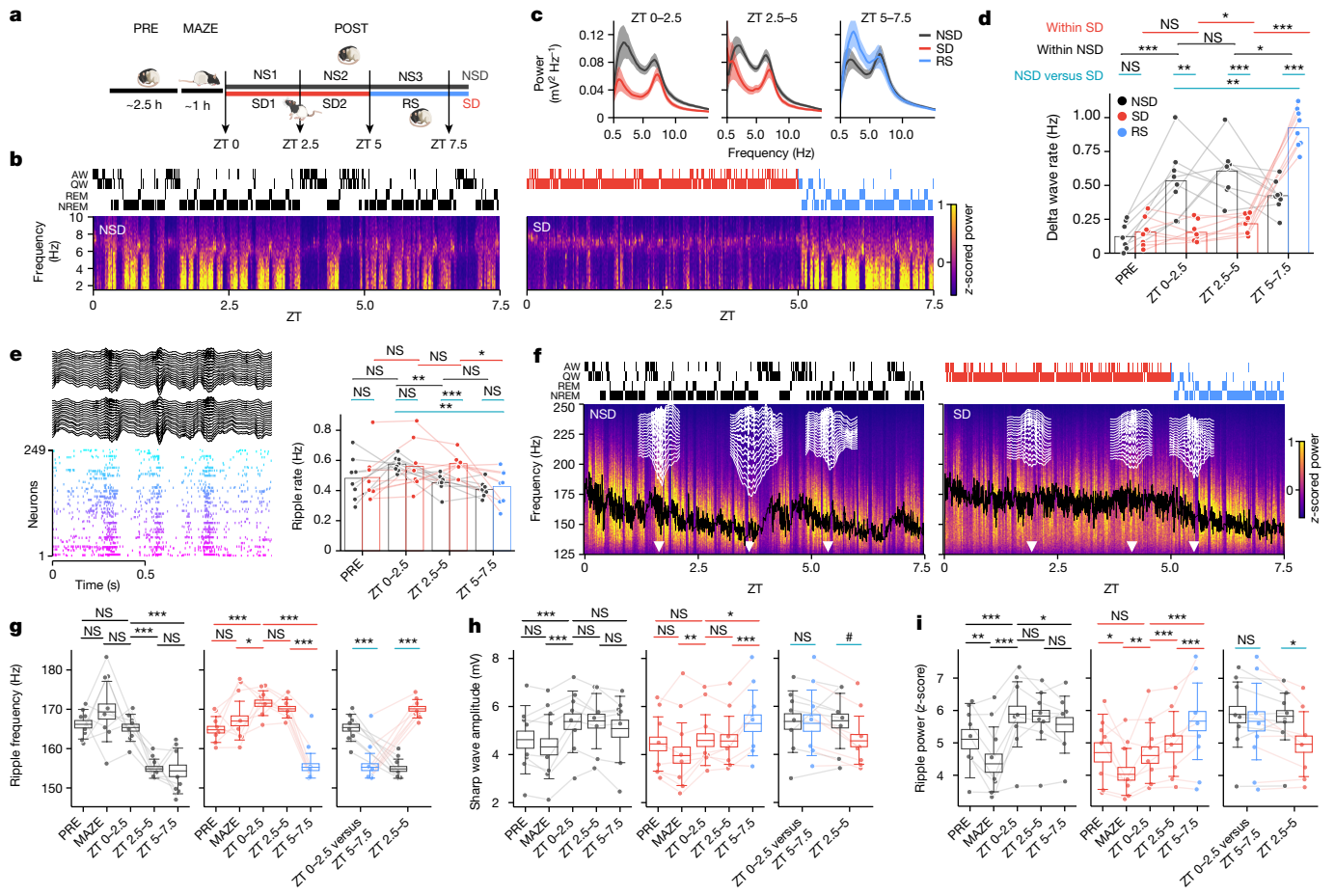


Fig. 1 | SD yields more SWRs but with weaker power and higher frequency ripples.

a, After PRE, animals were introduced to MAZE then allowed either undisturbed sleep (NS1–NS2) or 5 h of sleep deprivation (SD1–SD2) followed by recovery sleep (RS). **b**, Power spectral density in sample NSD (left) and SD (right) sessions with hypnogram (top) indicating brain state (active wake (AW), quiet wake (QW), REM and NREM sleep) and spectrogram (bottom; z-scored over all frequencies for the time periods shown) of CA1 cells LFP. **c**, Average power spectral densities across all NSD (black line with grey shading (s.e.m.); $n = 8$ sessions from 7 animals) and SD/RS sessions (red or blue line with corresponding shading (s.e.m.); $n = 8$ sessions from 7 animals). **d**, The rate of delta waves is lower during SD versus sleep but increases from SD1 to SD2 and RS (individual sessions superimposed with connected dots). **e**, Sample sleep (left) with a high spontaneous rate of SWRs with LFPs (two shanks in black) and unit rasters (arbitrary colour and sorting). The rate of SWRs (right) decreases with sleep but remains elevated during SD. **f**, Power spectral densities in

ripple frequency band for the sessions in **b** with moving average ripple frequency (black). Sample SWRs (16-channel traces, white) at different timepoints (arrow heads). **g**, Box plots showing population median and top/bottom quartiles (whiskers, $1.5 \times \text{IQR}$), estimated using HB, indicate higher frequency ripples in SD ($n = 157,964$ ripples total from eight sessions) versus NSD ($n = 143,681$ ripples total from eight sessions), with a rebound in RS. Session means overlaid as connected dots. Rightmost panel highlights cross-group comparisons for the first block of sleep in each group (NS1 versus RS) and the second block of SD versus NSD. **h, i**, Same as **g** for sharp-wave amplitude (**h**) and ripple band power (**i**). All panels, two-sided within-group comparisons and one-sided cross-group comparisons; **d, e**, t -tests; **g–i**, comparisons of bootstrapped means. NS, not significant; $^{\#}P < 0.10$, $^*P < 0.05$, $^{**}P < 0.01$, $^{***}P < 0.001$, with no corrections for multiple comparisons. See Supplementary Tables 1 and 2 for additional details. ZT, zeitgeber time.

relative to ad libitum sleep. SD sessions (eight sessions from seven animals) and NSD sessions (eight sessions from seven animals) were carried out in pseudo-random order on different days spaced more than 24 h apart, in the same animals.

Power spectral calculations (Fig. 1b,c) demonstrated strong delta (less than 4 Hz) power in the hippocampal LFP during non-rapid eye movement (NREM) sleep and strong theta (5–10 Hz) during rapid eye movement (REM) sleep (Extended Data Figs. 1 and 2a,b). We saw evidence for neither prominent delta during SD nor prominent theta outside REM periods²⁰. However, the rate of isolated delta waves (Fig. 1d) increased throughout the SD period, indicative of microsleep or local sleep^{21,22} (see Extended Data Fig. 2c for detected OFF states). Overall, SD was characterized by lower spectral power across frequencies (Fig. 1c). RS following SD subsequently featured a robust rebound in delta activity (Fig. 1c,d and Extended Data Figs. 1 and 2c), consistent with sleep homeostasis^{23,24}.

A higher rate of SWR during SD

Previous studies have suggested that the incidence rate of ripples and associated population burst events play important homeostatic roles in hippocampal dynamics^{16,17,25}. We therefore asked how the rate of these events changes during sleep compared to a similar period during extended wakefulness (Fig. 1e). In naturally sleeping animals, we found that the incidence rate of SWRs decreased over time, consistent with a homeostatic effect from sleep (NS1 median = 0.57 Hz (interquartile range (IQR) = 0.06 Hz) versus NS2 median = 0.46 Hz (IQR = 0.03 Hz), $P = 1.86 \times 10^{-3}$, paired t -test (d.f. = 7)). By contrast, the rate of SWRs remained high in animals during SD (SD1 median = 0.5 Hz (IQR = 0.16) versus SD2 median = 0.57 Hz (IQR = 0.03), $P = 0.73$, paired t -test (d.f. = 7)) and was higher during the second block (zeitgeber time = 2.5–5 h) of SD compared to NSD (SD2 versus NS2, $P = 1.08 \times 10^{-3}$, t -test (d.f.1 = 7 and d.f.2 = 7); Extended Data Fig. 2d,e). Once the SD

animals were allowed to sleep (at zeitgeber time = 5 h), the rate of ripples dropped to levels lower than those in the early block of ad libitum sleep (RS median = 0.45 Hz (IQR = 0.19) versus NS1 median = 0.57 Hz (IQR = 0.06), $P = 7.87 \times 10^{-3}$, *t*-test (d.f.1 = 7, and d.f.2 = 7)). In both NSD and SD, this ripple rate was consistently modulated by delta waves and the probability of an OFF state following a ripple increased over the course of SD (Extended Data Fig. 2f–j), as expected¹¹. Overall, the number of SWRs was not negatively affected but was higher during SD compared to natural sleep.

Sleep loss alters the physiological properties of SWR

Given the prevalence of SWRs during both sleep and sleep deprivation, we proposed that other characteristics of these hippocampal events might differ across these periods (Fig. 1f). The peak frequency of ripples in our recordings (Fig. 1g) decreased over the course of sleep (NS1 mean = 165.32 Hz (IQR = 1.75) versus NS3 mean = 154.37 Hz (IQR = 2.93), $P < 2 \times 10^{-4}$ (hierarchical bootstrap (HB) based on 10^4 random samples with replacement across data levels²⁶). However, during SD, ripple frequency remained elevated (SD2 mean = 170.13 Hz (IQR = 1.18) versus SD1 mean = 171.55 Hz (IQR = 1.58), $P = 0.14$, HB) and was significantly higher compared to ad libitum sleep, (SD2 mean versus NS2 mean = 154.87 Hz (IQR = 1.24), $P < 10^{-8}$, HB). The high frequency of ripples during SD (but not NSD) was also higher than those seen during MAZE ($P = 0.0204$, HB) or PRE sleep ($P < 10^{-4}$). Although changes in ripple frequency of the order of several Hz may be expected on the basis of temperature differences across sleep and awake²⁷, we observed larger differences of up to about 15 Hz (for example, SD2 versus NS2); these differences remained significant when accounting for state dependence (Extended Data Fig. 2k). After RS, ripple frequency dropped rapidly to levels lower than during the similar sleep period in NSD (RS mean = 155.40 Hz (IQR = 1.74) versus NS1 mean = 165.32 Hz (IQR = 1.75), $P = 3.54 \times 10^{-6}$, HB).

The sharp waves concurrent with ripples reflect synchronized Schaffer collateral input from CA3 converging on the apical dendrites of CA1 neurons. We measured changes in the amplitude of sharp waves using the difference between the most negative and most positive deflections (typically in stratum radiatum and stratum oriens, respectively) recorded on our CA1-spanning electrodes. In POST, we found increased amplitudes of sharp waves compared to MAZE in both NSD (NS1 mean = 5.36 mV (IQR = 0.65) versus MAZE mean = 4.33 mV (IQR = 0.67), $P < 2 \times 10^{-4}$, HB) and SD groups (SD1 mean = 4.62 mV (IQR = 0.53) versus MAZE mean = 4.00 mV (IQR = 0.67), $P = 1.40 \times 10^{-3}$, HB). These amplitudes were also larger than those observed during PRE for NSD (NS1 versus NSD PRE mean = 4.63 mV (IQR = 0.71), $P = 3 \times 10^{-4}$, HB) although not for SD (SD1 versus SD PRE mean = 4.45 mV (IQR = 0.57), $P = 0.13$, HB), including when accounting for state dependence (Extended Data Fig. 2k). Sharp-wave amplitudes did not change further over the course of NSD or SD (Fig. 1h) but RS elicited a strong increase in sharp-wave amplitudes (RS mean = 5.32 mV (IQR = 0.69) versus SD2 mean = 4.59 mV (IQR = 0.51), $P < 2 \times 10^{-4}$, HB). The power of ripples (100–250 Hz, z-scored over each entire session Fig. 1i) during SWRs varied similarly to sharp-wave amplitude, suggesting that higher amplitude sharp waves in the stratum radiatum produce stronger ripples in the pyramidal layer. These increased in POST relative to MAZE (NS1 mean = 5.88 mV (IQR = 0.51) versus MAZE mean = 4.39 mV (IQR = 0.56), $P < 10^{-4}$, HB) and SD1 mean = 4.64 (IQR = 0.50) versus MAZE mean = 4.06 mV (IQR = 0.39), $P = 1.8 \times 10^{-3}$, HB) and relative to PRE for NSD (NS1 mean = 5.88 mV (IQR = 0.50) versus PRE mean = 5.11 mV (IQR = 0.60), $P < 2 \times 10^{-4}$, HB) but not for SD (SD1 mean = 4.64 mV (IQR = 0.50) versus PRE mean = 4.72 mV (IQR = 0.59), $P = 0.65$, HB) (Extended Data Fig. 2k). Ripple power (z-scored over the session) then decreased over the course of sleep (NS3 mean = 5.57 (IQR = 0.44) versus NS1 mean = 5.88 (IQR = 0.50), $P = 1.8 \times 10^{-2}$, HB) but increased over SD (SD2 mean = 4.97 (IQR = 0.50) versus SD1 mean = 4.64 (IQR = 0.50), $P < 2 \times 10^{-4}$, HB) and even further after RS (RS mean = 5.67 (IQR = 0.59), $P < 2 \times 10^{-4}$, HB). Although these measures showed high variability across subjects, cross-group

comparisons (NS2 mean versus SD2 mean) were significant for ripple power ($P = 0.040$) and demonstrated a trend for sharp-wave amplitude ($P = 0.090$). Overall, these results demonstrate that, although the total number of ripples remains elevated during SD, sleep loss manifests with higher frequency ripples but at lower power and with smaller sharp waves, potentially reflecting the physiological impact of fatigue on the pyramidal cell–interneuron interactions that give rise to these events²⁸.

Sleep loss disturbs firing-rate dynamics in the hippocampal network

The firing rates of neurons are sensitive to changes in sleep states²⁹, serve as important signals of the homeostatic function of sleep^{25,30} and can reflect the strength of synaptic connectivity among neurons^{17,30}. We therefore assessed the effects of sleep and sleep loss on hippocampal firing-rate dynamics (Fig. 2). During active exploration of the maze, firing rates tended to increase from PRE for pyramidal cells (NSD in which MAZE mean = 1.15 Hz (IQR = 0.14) versus PRE mean = 0.94 Hz (IQR = 0.14), $P = 0.0028$, HB; but not significantly for SD in which MAZE mean = 1.11 Hz (IQR = 0.26) versus PRE mean = 0.95 Hz (IQR = 0.21), $P = 0.128$, HB) and for interneurons (a trend for NSD with MAZE mean = 23.35 Hz (IQR = 4.30) versus PRE mean = 20.34 Hz (IQR = 5.23), $P = 0.055$, HB; and significantly for SD with MAZE mean = 21.96 Hz (IQR = 3.88) versus PRE mean = 18.72 Hz (IQR = 4.12), $P = 0.044$, HB). However, following MAZE, sleep loss produced different dynamics from natural sleep. Pyramidal cell firing rates (Fig. 2a,b) dropped significantly within hours of natural sleep (NS1 mean = 0.90 Hz (IQR = 0.12) versus MAZE, $P = 0.028$, HB) and further over the course of NSD (NS2 mean = 0.80 Hz (IQR = 0.09) versus NS1, $P = 2.8 \times 10^{-3}$, HB) but they remained elevated throughout the 5 h SD period (SD2 mean = 1.04 Hz (IQR = 0.23) versus SD1 mean = 1.01 Hz (IQR = 0.20), $P = 0.55$, HB). Differences were also evident in the distributions of pyramidal cell firing rates; these were skewed during PRE and MAZE, subsequently became log-normal in sleep^{29,31} but remained skewed in SD (NS2 mean IQR = 0.63 log(Hz), $P = 0.24$, versus SD2 mean IQR = 0.81 log(Hz), $P = 2.7 \times 10^{-3}$, HB of Shapiro–Wilk test, Fig. 2d), with a broader distribution (Fig. 2e). These broad and negatively skewed distributions indicate that during prolonged awake SD a few cells fire at elevated rates whereas other reduce firing, suggestive of competition among neurons mediated by inhibition²⁹. Consistent with this, interneuron firing rates (Fig. 2c) decreased with the onset of natural sleep and remained so throughout sleep (NS1 mean = 17.91 Hz (IQR = 3.37) versus MAZE mean = 23.35 Hz (IQR = 4.30), $P = 4 \times 10^{-4}$, HB; NS3 mean = 16.86 Hz (IQR = 3.02) versus NS1, $P = 0.21$, HB) but, in contrast, remained elevated from MAZE to SD (SD1 mean = 20.28 Hz (IQR = 5.32) versus MAZE mean = 21.96 Hz (IQR = 3.88), $P = 0.34$, HB) and the remainder of SD (SD2 mean = 20.03 Hz (IQR = 5.01) versus SD1, $P = 0.66$, HB). With the onset of RS, firing rates decreased rapidly for pyramidal cells (RS mean = 0.72 Hz (IQR = 0.19) versus SD2 mean = 1.04 Hz (IQR = 0.22), $P < 2 \times 10^{-4}$, HB) and interneurons (RS mean = 13.02 Hz (IQR = 3.41) versus SD2 mean = 20.03 (IQR = 5.01), $P < 2 \times 10^{-4}$, HB). Owing to large variability, cross-group comparisons were less salient but demonstrated a trend towards higher firing rates in pyramidal cells in the second block of SD compared to NSD (NS2 mean = 0.80 Hz (IQR = 0.09) versus SD2 mean = 1.04 Hz (IQR = 0.22) $P = 0.074$). Interneurons likewise trended towards lower firing rates in natural sleep compared to RS (NS1 mean = 17.91 Hz (IQR = 3.37) versus RS mean = 13.03 Hz (IQR = 3.47), $P = 0.090$, HB). Although these patterns were largely attributable to state-dependent effects of waking and NREM (Extended Data Fig. 3), overall, the increased firing rates and skewed distributions in SD compared to ad libitum natural sleep indicate a higher metabolic impact of prolonged waking on hippocampal activities, which confirm and extend previous observations^{25,29}.

Interneurons of different types have a variety of firing response during SWRs and play an important role in determining the physiological characteristics of the ripple oscillation. Therefore, we also examined the firing responses of interneurons, alongside those of pyramidal

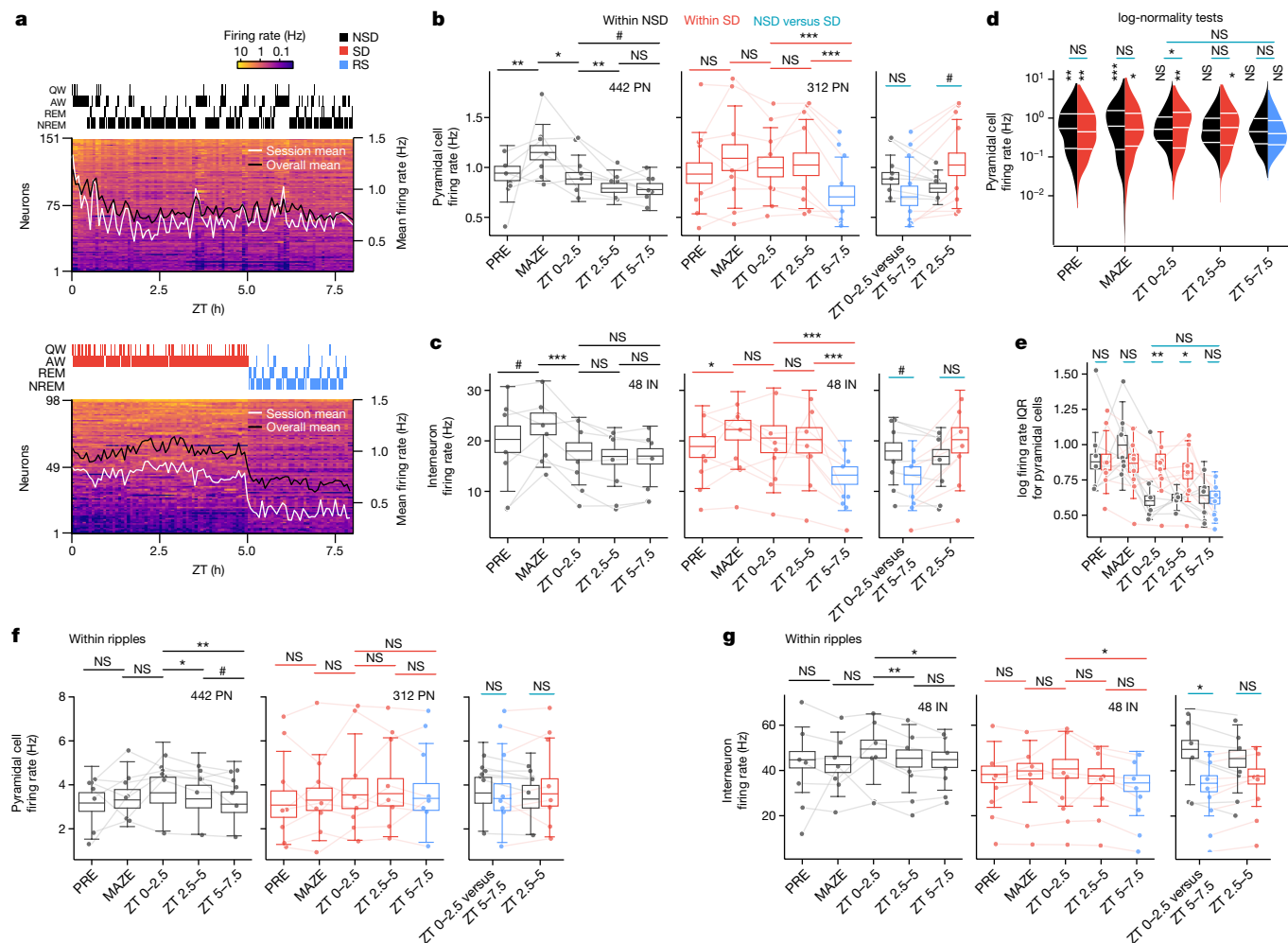


Fig. 2 | Hippocampal firing rates are elevated and more dispersed during SD. **a**, Example sessions from NSD (top) and SD (bottom) with RS, showing firing rates of pyramidal units (5 min bins, units sorted by mean) and hypnograms (top: AW, QW, REM and NREM sleep) during POST. Mean firing rate (right axis) superimposed (white, this session; black, across all sessions). **b**, Pyramidal neurons (PNs) during NSD (black, left; $n = 442$ cells from eight sessions) and SD/RS (red/blue, right; $n = 312$ cells from eight sessions) in (PRE, MAZE, ZT 0–2.5, ZT 2.5–5 and ZT 5–7.5) show decreasing firing during sleep but elevated firing during SD. Individual session means superimposed (connected dots). **c**, Same as **b** but for interneurons (IN) ($n = 48$ cells from eight NSD sessions and $n = 48$ cells from eight SD sessions). **d**, The full distribution of PN firing rates deviates from log-normal during SD1 and SD2 but not NS1 or NS2.

e, log firing rate IQR shows greater variance for PNs in SD versus NSD. **f**, PN firing rates specifically in ripples decreased over sleep and remained stable during SD but with minimal cross-group differences. **g**, IN firing during ripples decreased over sleep but remained elevated during SD then dropped in RS, with significant differences between NS1 and RS. All box plots depict median and top and bottom quartiles (whiskers, $1.5 \times$ IQR) of the HB data. **b, c, e–g**, two-sided within-group comparisons and one-sided cross-group comparisons of HB means. **d**, Shapiro–Wilk tests performed on each HB log distribution, with P obtained from the proportion with significant skew; one-sided cross-group comparisons performed on the HB Shapiro–Wilk test statistics. # $P < 0.10$, * $P < 0.05$, ** $P < 0.01$, *** $P < 0.001$, with no corrections for multiple comparisons. See Supplementary Table 1 for additional details.

cells, specifically in SWRs (Fig. 2f,g). Although firing rates in ripples varied across the periods we examined, we generally saw little difference between natural sleep and SD (pyramidal neurons having NS2 mean = 3.44 Hz (IQR = 1.03) versus SD2 mean = 3.71 Hz (IQR = 1.24), $P = 0.41$, HB; interneurons having NS2 mean = 45.16 Hz (IQR = 7.36) versus SD2 mean = 37.38 Hz (IQR = 6.61), $P = 0.16$, HB). However, we observed a significant decrease in the ripple firing rates of interneurons during RS compared to the similar period in natural sleep (RS mean = 34.11 Hz (IQR = 7.11) versus NS1 mean = 49.37 Hz (IQR = 7.85), $P = 0.033$, HB). Somatostatin-positive interneurons, a subset of which are lacunosum moleculare-projecting interneurons which gate entorhinal cortical input to CA1 (ref. 32), generally fire at lower rates during SWRs than do other cells³³. The lowered firing rates we observe during RS may therefore reflect the differential impact of sleep loss specifically on this class of interneurons, consistent with a recent study using immediate early genes³⁴.

Sleep loss attenuates memory reactivation

Given that our results thus far demonstrate a high rate of SWRs during SD with robust concurrent firing in pyramidal cells, we next asked whether the specific content of SWRs may be impacted by SD. We first examined the reactivation of neuronal ensembles, which have been linked to the memory function of the hippocampus^{2,18}. Such reactivations can persist for hours after a new experience³⁵ and can broadcast the hippocampal signal to cortical regions^{2,8,9}. To quantify reactivation, we calculated the partial correlation explained variance (EV) (Methods), which measures the similarity of pairwise correlations between MAZE and POST while controlling for pre-existing correlations in PRE³⁶ in 250 ms bins in sliding 15 min windows (5 min steps; Fig. 3a). A time-reversed explained variance (REV) was used to estimate the chance level for reactivation³⁷. In naturally sleeping animals following exposure to the new maze we observed hours-long reactivation, consistent with

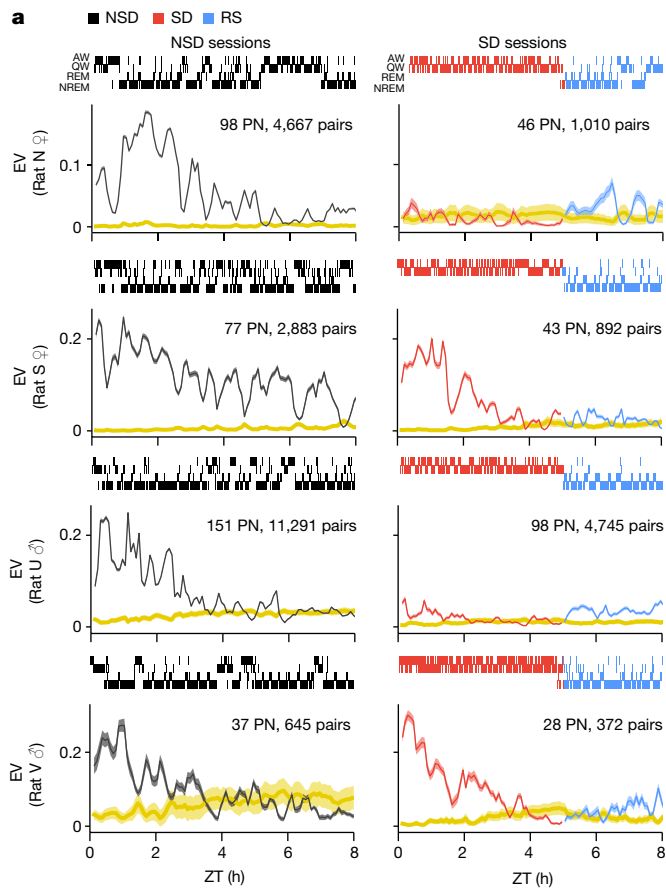
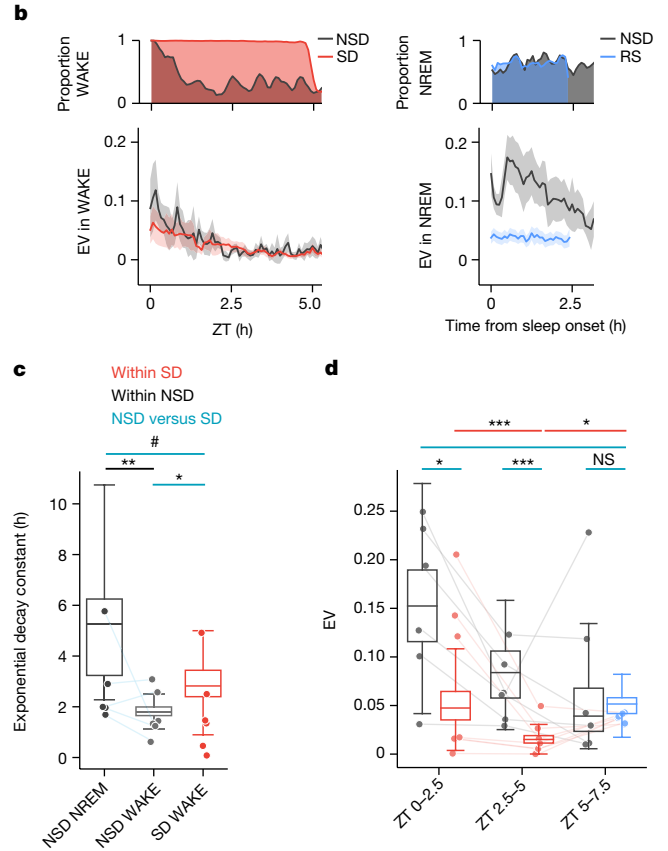


Fig. 3 | Reactivation attenuates during SD and is not restored by RS. a, EV of pairwise reactivation (NSD, black; SD, red) and its chance levels (REV, yellow (maize)) during POST in ad libitum sleep (NSD; left column) and SD with RS (right column) sessions from four animals (sex on y axis; hypnogram on top (AW, QW, REM and NREM sleep); additional sessions in Extended Data Fig. 4). Solid line shows mean EV/REV and shaded regions indicate low standard deviations. NSD sessions featured robust reactivation lasting for hours, whereas SD sessions showed either some (rats S and V) or little reactivation (rats N and U). **b**, Proportion of time spent in WAKE during NSD and SD (top left) and in NREM during NSD and RS (top left). When calculated exclusively during WAKE (bottom left), mean EV (mean and s.d. are shown by solid line and shading, respectively) shows a similar decrease in both NSD ($n = 20,544$ cell pairs from six sessions) and SD ($n = 8,114$ cell pairs from seven sessions),

our previous study³⁵. During SD, however, we observed one of two scenarios: either virtually no reactivation (for example, rats N and U, Fig. 3a; seen in four of seven sessions, Extended Data Fig. 4) or reactivation similar to NSD but with a faster rate of decay (for example, rats S and V, Fig. 3a; seen in three of seven sessions, Extended Data Fig. 4). These differences were not caused by discrepancies in the amount of time or the distance covered on the MAZE or in the proportion of active versus quiet wake states in the home cage (Extended Data Fig. 5a–c). However, we observed a significant negative correlation ($r = -0.9$, $P = 0.006$, Pearson correlation coefficient) between the rate of delta waves during SD2 (Extended Data Fig. 5d but not during other periods) and the amount of reactivation (EV) during SD1. Given that delta waves represent accumulated sleep pressure^{21,38}, this indicates that variations in sleepiness or resilience to sleep loss could potentially explain the differences in the capacity for hippocampal reactivation in sleep-deprived animals³⁹.

Overall, when we compared EV calculated exclusively during the awake state (Fig. 3b, left), we found similarly low levels of reactivation which decreased over time in both NSD and SD, in contrast to the higher



but when calculated exclusively during NREM (bottom right), there is lower reactivation in RS than in NSD. **c**, The decay constant obtained from exponential fits to EV curves separated by brain state (individual sessions overlaid with connected dots, except for out of range). In NSD, EV decays more slowly during NREM versus WAKE. The WAKE EV decays more slowly in SD compared to NSD but trends towards faster decay than during NSD NREM. **d**, EV plots indicate lower reactivation during SD versus NSD, with a rebound during RS to lower levels than in ad libitum sleep. All box plots depict median and top and bottom quartiles (whiskers, $1.5 \times$ IQR) of HB data. Two-sided within-group comparisons and one-sided cross-group comparisons of bootstrapped means, $^{\#}P < 0.1$, $^*P < 0.05$, $^{**}P < 0.01$, $^{***}P < 0.001$, with no corrections for multiple comparisons. See Supplementary Table 1 for additional details.

reactivation during sleep exclusively in NSD (Fig. 3b, right). Across subjects, the time constant of decay, estimated from an exponential fit to EV, was significantly larger in NREM compared to waking NSD (Fig. 3c) and also larger in waking SD than in waking NSD, suggestive of compensation for the lack of sleep in the former group. Reactivation levels were significantly lower during SD (Fig. 3d) when comparing SD1 with NS1 as well as comparing SD2 with NS2. Thus, compared to sleep, the awake state demonstrated a more limited capacity for reactivation. Prolonged waking, in particular, provided a lower level of reactivation when compared to ad libitum sleep during the same period. However, although reactivation was nearly absent by the end of SD, it increased significantly with the onset of RS (Fig. 3a,d). This suggests that the hippocampus is capable of reprising ensemble patterns reactivation even after a pause, such as during SD. But critically, even with this compensatory increase, reactivation levels during RS were substantially reduced compared to a corresponding period from NSD (Fig. 3b,d; see also comparisons for 1 h blocks in Extended Data Fig. 6). This reveals a persisting consequence of SD that, unlike other effects of sleep loss, is not restored even after lost sleep is reclaimed.

Sequence replay deteriorates during SD and RS

Whereas pairwise measures, such as EV, measure neuronal reactivation, finer scale analysis has revealed that neuronal activity during SWRs can also provide a temporally compressed replay of sequences of place cells which fired during maze behaviour^{2,18}. Although most studies of replay have been directed at rest and sleep within an hour of maze exposure, we took advantage of our long-duration recordings to investigate how replay (Fig. 4a) unfolds over several hours of sleep compared with SD. As quantification of these events relies on different assumptions about the nature of replay^{40,41}, we focused on using Bayesian methods (Fig. 4b) to simply quantify the proportion of ripple events that decode continuous movement through the maze (trajectory replays). Ripple events featuring five or more active units during animal movement speeds of less than 8 cm s⁻¹ and peak ripple power of more than 1 s.d. were considered candidates for further analyses (Methods). We assessed trajectory structure using the distance between decoded locations in adjacent time steps, referred to as 'jump distance'⁴²; ripple events with jump distance less than 40 cm in at least three consecutive time bins, were classified as trajectory replays.

We observed that the proportion of ripples qualifying as trajectory replays was highest on the maze in both experimental groups and was also higher in ad libitum sleep in NS1 compared to PRE (Extended Data Fig. 7), consistent with previous reports^{43,44}. However, the proportion of trajectory replays significantly decreased over the course of SD (SD1 mean = 0.21 (IQR = 0.034) versus SD2 mean = 0.018 (IQR = 0.028), $P = 0.024$, HB) and was significantly lower from natural ad libitum sleep by the second block of SD (NS2 mean \pm s.e.m. = 0.26 (IQR = 0.017) versus SD2 mean = 0.018 (IQR = 0.18), $P = 4.02 \times 10^{-4}$). Even during RS, replays decreased further and did not rebound to the comparative levels in NSD (Fig. 4c; RS mean = 0.016 (IQR = 0.023) versus NS1 mean = 0.027 (IQR = 0.034), $P = 1.98 \times 10^{-4}$, HB). The total rate of trajectory replays (Fig. 4d) was also lower in the first block of SD compared to NSD (SD1 mean = 590 (IQR = 84) versus NS1 mean = 840 (IQR = 128), $P = 0.014$, HB) and remained significantly lower in RS (RS mean = 290 (IQR = 64) versus NS1 mean = 840 (IQR = 128), $P < 10^{-4}$, HB). Although the patterns in the effects of SD/RS versus NSD on trajectory replays somewhat differ from those for reactivation, some discrepancies are expected because of the methodological differences in the measures used for these patterns⁴¹. Further differences could also arise if pairwise co-activations during sleep reflect the maze experience without integrating into neural sequences that correspond to paths with momentum through the maze environment⁴⁵⁻⁴⁷.

Finally, motivated by a recent study that reported a memory benefit for longer replays⁷, we measured and compared the durations of trajectory replays (Fig. 4e). Although we did not detect significant cross-group differences in replay durations, within SD (but not NSD) we observed a significant decrease from the first to the second block (SD1 mean 0.203 s (IQR = 0.0097 s) versus SD2 mean = 0.186 s (IQR = 0.013 s), $P < 2 \times 10^{-4}$, HB) and a further decrease in RS (SD2 mean = 0.186 s (IQR = 0.013 s) versus RS mean = 0.172 s (IQR = 0.014 s), $P = 0.012$, HB). Overall, these results demonstrate that the loss of sleep immediately following a new experience diminishes the hippocampal replay of place cell patterns following new maze exposure and that this impairment persists even when sleep is regained.

Discussion

During sleep deprivation compared to natural sleep, we observed lower amplitude sharp waves coupled with lower power ripples and higher frequency ripple oscillations at the CA1 pyramidal layer. Higher amplitude and power generally indicate greater synchrony of CA3 inputs to CA1 neurons, leading to greater spiking in CA1 neurons^{2,48} and stronger resonance throughout the hippocampal formation⁸, although the animals' sleep/awake states were not separated in most of these

studies. Nevertheless, one recent study reported that SWRs during waking, for which we observe lower power ripples, have a larger impact on prefrontal cortical neurons⁴⁹ than they do during sleep. Similarly, another study reported that lower amplitude sharp waves produced larger neuronal responses in extra-hippocampal regions⁸. These observations suggest that larger sharp waves do not necessarily translate to greater activation in target regions. Additionally, hippocampal firing rates during SWRs remained comparable between sleep-deprived and sleeping animals despite differences in SWR features, indicating that SWRs of different power and amplitude can generate similar responses in hippocampal neurons.

The increase in ripple power over SD but decrease in power over sleep, with parallel changes in ripple frequency, suggest that these SWR features can serve as indicators of sleep pressure. These indicators are measurable from the hippocampal LFP in both waking and sleep, in contrast to cortical slow-wave activity used in common models of sleep homeostasis²⁴, which can only be measured during sleep (see also ref. 23). Higher frequency ripples potentially reflect the higher metabolism of the awake state⁵⁰ which is progressively lowered and reset in sleep²⁵. However, differences in ripple frequency can also reflect differential neuromodulatory tone, such as activation of GABA-A⁵¹ or 5-HT receptors⁵², or different routing of inputs to CA1, with higher frequency ripples reflecting the influence of CA2 during waking⁵³ and lower frequency ripples reflecting input from the entorhinal cortex^{2,54}. Consistent with this notion, we noted an increase in ripple frequency, coupled with higher power and higher amplitude sharp waves, following the new maze exposure, particularly in the awake state (Extended Data Fig. 2k; see also ref. 55). Lower frequency ripples have also been associated with aging⁵⁶, whereas ripple frequency increases after learning⁵⁷, consistent with the postulated correlation with higher metabolic cost.

In addition to differences in physiological features of SWRs, we reported firing-rate patterns that seem generally consistent with the 'synaptic homeostasis hypothesis'^{25,50}, which conjectures that waking drives strengthened connectivity between neurons, whereas sleep drives synaptic downscaling. The decrease in reactivation and replay over the course of sleep may likewise be consistent with this hypothesis as the pathways providing reverberation of waking patterns are progressively reduced. On the other hand, the more rapid decline in replay and reactivation during SD versus sleep is not readily reconciled with a privileged role for waking in synaptic strengthening. If synaptic strengthening indeed occurs preferentially during the awake state, then it could be expected to elicit more robust reactivation than during sleep. Another possibility, however, is that the strengthening during awake activity is promiscuous rather than specific to the firing patterns evidenced on the maze. In this scenario, waking during SD may actively interfere with hippocampal reactivation by provoking the hippocampus to generate and learn new patterns inconsistent with the maze experience. Similarly, whereas it has been conjectured that SWRs may serve to downscale synapses^{17,25,50}, reactivation and replay were longer lasting during sleep, even though SD featured a higher incidence rate of SWRs, potentially indicating a homeostatic drive⁵⁸. The background brain states against which SWRs occur, along with the specific hippocampal firing patterns that they produce, probably play an important role in determining their effects on the hippocampal circuit and other brain regions^{6,8,17,49}.

Notably, in this study we found reactivation during natural sleep that lasted for hours³⁵ but diminished reactivation during SD with only limited rebound when animals eventually regained lost sleep. The absence of a more complete rebound was remarkable because although most indices of brain health and function, including protein signalling⁵⁹ and gene transcription⁶⁰, return to normal levels following sufficient RS, memories compromised by sleep loss typically do not recover^{3,59,60}. Overall, our work calls attention to reactivation and replay, rather than simply the occurrence of SWRs, as potentially the crucial elements that mediate the role of sleep in memory and the negative impact of sleep

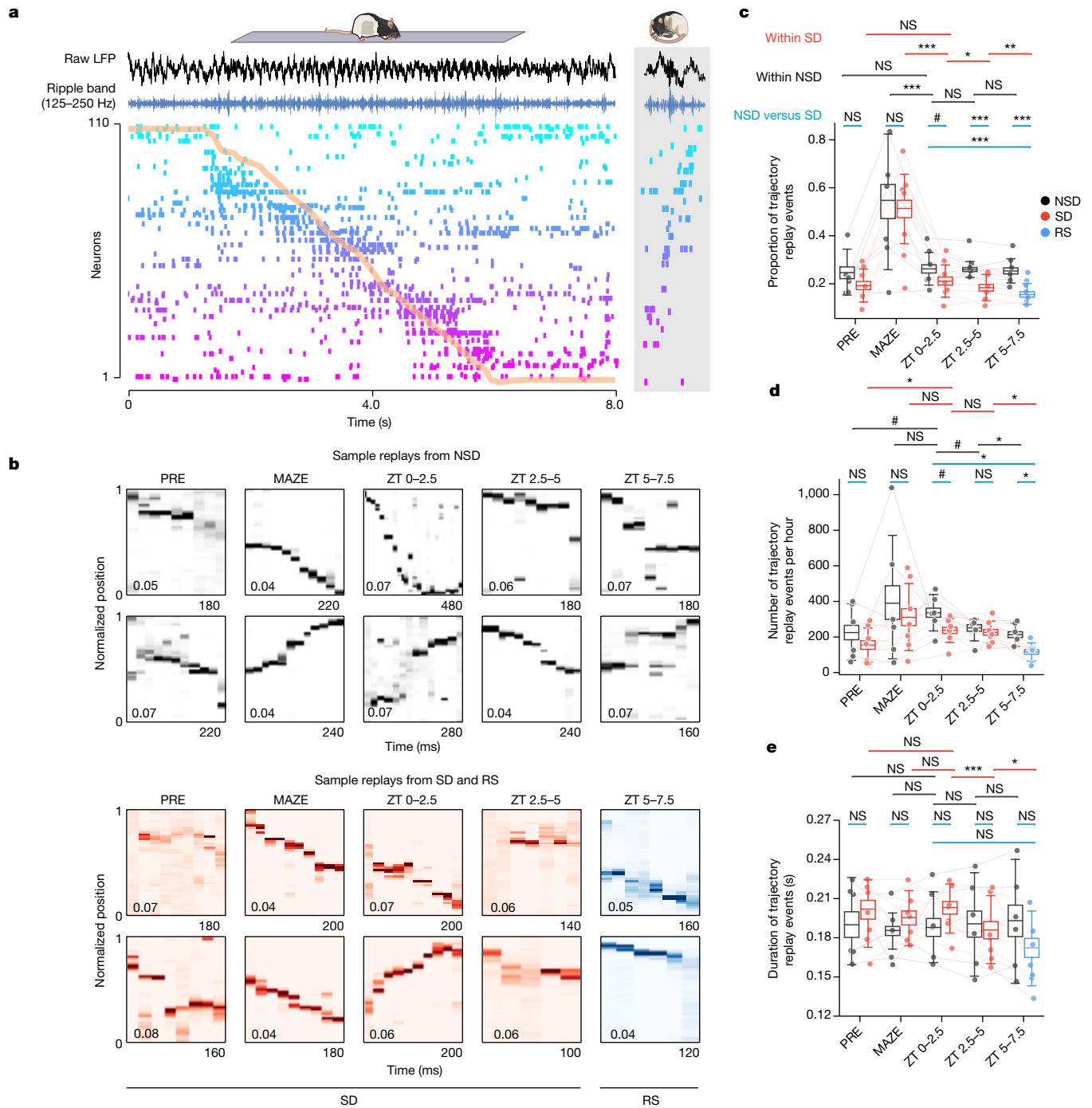


Fig. 4 | Trajectory replays deteriorate over SD and RS. **a**, Hippocampal spike raster (arbitrary colours ordered by place field location) and raw (black) and ripple-filtered (blue) local field (LFP) during a sample run (normalized track position overlaid in orange). Grey box (right) shows a sample sleep replay. **b**, Sample trajectory replays for NSD and SD from top 10 percentile of distance covered and lowest 10 percentile of mean jump distance (value in lower left of each box gives the normalized distance) in each epoch. Replays were observed in all epochs but became progressively shorter, particularly in SD, with fewer events meeting the replay criteria. **c**, Fewer events qualified as replays by the second block of SD ($n = 72,584$ candidate events from seven sessions) and in RS compared to NSD (of $n = 64,205$ candidate events from six sessions). Critically, the proportion of replays in RS was significantly lower than in the

equivalent period from ad libitum sleep (NS1). **d**, Similar to **c** but for the rate of replays. Fewer replays were seen in the first block of SD compared to NSD and there were fewer replays in RS versus NS1. **e**, The durations of trajectory replays were significantly reduced from the first to second block of SD ($n = 15,005$ replays from seven sessions) but not NSD ($n = 17,742$ replays from six sessions), with a further decrease after RS. All box plots depict median and top and bottom quartiles (whiskers, $1.5 \times$ IQR) of the HB data with individual session means overlaid and connected. Two-sided within-group comparisons and one-sided cross-group comparisons of bootstrapped means; $^{\#}P < 0.1$, $^*P < 0.05$, $^{**}P < 0.01$, $^{***}P < 0.001$, with no corrections for multiple comparisons. See Supplementary Table 1 for additional details.

loss. The disruption of these neuronal firing patterns could destabilize hippocampal spatial representations^{19,47} and hippocampus-dependent spatial memories⁶. Furthermore, as SWRs provide privileged windows

of communication between the hippocampus and other brain regions¹¹, the compromised nature of this exchange is likely to have repercussions on networks distributed throughout the brain^{8,9}.

Online content

Any methods, additional references, Nature Portfolio reporting summaries, source data, extended data, supplementary information, acknowledgements, peer review information; details of author contributions and competing interests; and statements of data and code availability are available at <https://doi.org/10.1038/s41586-024-07538-2>.

- Rasch, B. & Born, J. About sleep's role in memory. *Physiol. Rev.* **93**, 681–766 (2013).
- Buzsaki, G. Hippocampal sharp wave-ripple: a cognitive biomarker for episodic memory and planning. *Hippocampus* **25**, 1073–1188 (2015).
- Havekes, R. & Abel, T. The tired hippocampus: the molecular impact of sleep deprivation on hippocampal function. *Curr. Opin. Neurobiol.* **44**, 13–19 (2017).
- Eschenko, O., Ramadan, W., Mölle, M., Born, J. & Sara, S. J. Sustained increase in hippocampal sharp-wave ripple activity during slow-wave sleep after learning. *Learn. Mem.* **15**, 222–228 (2008).
- Girardeau, G., Benchenane, K., Wiener, S. I., Buzsaki, G. & Zugaro, M. B. Selective suppression of hippocampal ripples impairs spatial memory. *Nat. Neurosci.* **12**, 1222–1223 (2009).
- Gridchyn, I., Schoenenberger, P., O'Neill, J. & Csicsvari, J. Assembly-specific disruption of hippocampal replay leads to selective memory deficit. *Neuron* **106**, 291–300 (2020).
- Fernandez-Ruiz, A. et al. Long-duration hippocampal sharp wave ripples improve memory. *Science* **364**, 1082–1086 (2019).
- Nitzan, N., Swanson, R., Schmitz, D. & Buzsaki, G. Brain-wide interactions during hippocampal sharp wave ripples. *Proc. Natl Acad. Sci. USA* **119**, e2200931119 (2022).
- Logothetis, N. K. et al. Hippocampal–cortical interaction during periods of subcortical silence. *Nature* **491**, 547–553 (2012).
- Karimi Abadchi, J. et al. Spatiotemporal patterns of neocortical activity around hippocampal sharp-wave ripples. *eLife* **9**, e51972 (2020).
- Rothschild, G. The transformation of multi-sensory experiences into memories during sleep. *Neurobiol. Learn. Mem.* **160**, 58–66 (2019).
- Nere, A., Hashmi, A., Cirelli, C. & Tononi, G. Sleep-dependent synaptic down-selection (I): modeling the benefits of sleep on memory consolidation and integration. *Front. Neurol.* **4**, 143 (2013).
- Tadros, T., Krishnan, G. P., Ramya, R. & Bazhenov, M. Sleep-like unsupervised replay reduces catastrophic forgetting in artificial neural networks. *Nat. Commun.* **13**, 7742 (2022).
- King, C., Henze, D. A., Leinekugel, X. & Buzsaki, G. Hebbian modification of a hippocampal population pattern in the rat. *J. Physiol.* **521**, 159–167 (1999).
- Sadowski, J. H., Jones, M. W. & Mellor, J. R. Sharp-wave ripples orchestrate the induction of synaptic plasticity during reactivation of place cell firing patterns in the hippocampus. *Cell Rep.* **14**, 1916–1929 (2016).
- Colgin, L. L., Kubota, D., Jia, Y., Rex, C. S. & Lynch, G. Long-term potentiation is impaired in rat hippocampal slices that produce spontaneous sharp waves. *J. Physiol.* **558**, 953–961 (2004).
- Norimoto, H. et al. Hippocampal ripples down-regulate synapses. *Science* **359**, 1524–1527 (2018).
- Joo, H. R. & Frank, L. M. The hippocampal sharp wave-ripple in memory retrieval for immediate use and consolidation. *Nat. Rev. Neurosci.* **19**, 744–757 (2018).
- Roux, L., Hu, B., Eichler, R., Stark, E. & Buzsaki, G. Sharp wave ripples during learning stabilize the hippocampal spatial map. *Nat. Neurosci.* **20**, 845–853 (2017).
- Ognjanovski, N., Broussard, C., Zochowski, M. & Aton, S. J. Hippocampal network oscillations rescue memory consolidation deficits caused by sleep loss. *Cereb. Cortex* **28**, 3711–3723 (2018).
- Vyazovskiy, V. V. et al. Local sleep in awake rats. *Nature* **472**, 443–447 (2011).
- Friedman, L., Bergmann, B. M. & Rechtschaffen, A. Effects of sleep deprivation on sleepiness, sleep intensity and subsequent sleep in the rat. *Sleep* **1**, 369–391 (1979).
- Thomas, C. W., Guillaumin, M. C., McKillop, L. E., Achermann, P. & Vyazovskiy, V. V. Global sleep homeostasis reflects temporally and spatially integrated local cortical neuronal activity. *eLife* **9**, e54148 (2020).
- Borbely, A. A. & Achermann, P. Sleep homeostasis and models of sleep regulation. *J. Biol. Rhythms* **14**, 557–568 (1999).
- Miyawaki, H. & Diba, K. Regulation of hippocampal firing by network oscillations during sleep. *Curr. Biol.* **26**, 893–902 (2016).
- Saravanan, V., Berman, G. J. & Sober, S. J. Application of the hierarchical bootstrap to multi-level data in neuroscience. *Neuron. Behav. Data Anal. Theory*. Preprint at <https://arxiv.org/abs/2007.07797> (2020).
- Petersen, P. C., Voroslakos, M. & Buzsaki, G. Brain temperature affects quantitative features of hippocampal sharp wave ripples. *J. Neurophysiol.* **127**, 1417–1425 (2022).
- Stark, E. et al. Pyramidal cell–interneuron interactions underlie hippocampal ripple oscillations. *Neuron* **83**, 467–480 (2014).
- Miyawaki, H., Watson, B. O. & Diba, K. Neuronal firing rates diverge during REM and homogenize during non-REM. *Sci. Rep.* **9**, 689 (2019).
- Torrado Pacheco, A., Böttorff, J., Gao, Y. & Turrigiano, G. G. Sleep promotes downward firing rate homeostasis. *Neuron* **109**, 530–544 (2021).
- Mizuseki, K. & Buzsaki, G. Preconfigured, skewed distribution of firing rates in the hippocampus and entorhinal cortex. *Cell Rep.* **4**, 1010–1021 (2013).
- Leao, R. N. et al. OLM interneurons differentially modulate CA3 and entorhinal inputs to hippocampal CA1 neurons. *Nat. Neurosci.* **15**, 1524–1530 (2012).
- Royer, S. et al. Control of timing, rate and bursts of hippocampal place cells by dendritic and somatic inhibition. *Nat. Neurosci.* **15**, 769–775 (2012).
- Delorme, J. et al. Sleep loss drives acetylcholine- and somatostatin interneuron-mediated gating of hippocampal activity to inhibit memory consolidation. *Proc. Natl Acad. Sci. USA* **118**, e2019318118 (2021).
- Giri, B., Miyawaki, H., Mizuseki, K., Cheng, S. & Diba, K. Hippocampal reactivation extends for several hours following novel experience. *J. Neurosci.* **39**, 866–875 (2019).
- Kudrimoti, H. S., Barnes, C. A. & McNaughton, B. L. Reactivation of hippocampal cell assemblies: effects of behavioral state, experience and EEG dynamics. *J. Neurosci.* **19**, 4090–4101 (1999).
- Pennartz, C. M. et al. The ventral striatum in off-line processing: ensemble reactivation during sleep and modulation by hippocampal ripples. *J. Neurosci.* **24**, 6446–6456 (2004).
- Franken, P., Chollet, D. & Tafti, M. The homeostatic regulation of sleep need is under genetic control. *J. Neurosci.* **21**, 2610–2621 (2001).
- Lee, A., Lei, H., Zhu, L., Jiang, Z. & Ladiges, W. Resilience to acute sleep deprivation is associated with attenuation of hippocampal mediated learning impairment. *Aging Pathobiol. Ther.* **2**, 195–202 (2020).
- van der Meer, M. A. A., Kemere, C. & Diba, K. Progress and issues in second-order analysis of hippocampal replay. *Philos. Trans. R Soc. Lond. B* **375**, 20190238 (2020).
- Tingley, D. & Peyrache, A. On the methods for reactivation and replay analysis. *Philos. Trans. R Soc. Lond. B* **375**, 20190231 (2020).
- Silva, D., Feng, T. & Foster, D. J. Trajectory events across hippocampal place cells require previous experience. *Nat. Neurosci.* **18**, 1772–1779 (2015).
- Grosmark, A. D. & Buzsaki, G. Diversity in neural firing dynamics supports both rigid and learning hippocampal sequences. *Science* **351**, 1440–1443 (2016).
- Farooq, U., Sibille, J., Liu, K. & Dragoi, G. Strengthened temporal coordination within pre-existing sequential cell assemblies supports trajectory replay. *Neuron* **103**, 719–733 (2019).
- Stella, F., Baracska, P., O'Neill, J. & Csicsvari, J. Hippocampal reactivation of random trajectories resembling Brownian diffusion. *Neuron* **102**, 450–461 (2019).
- Krause, E. L. & Drugowitsch, J. A large majority of awake hippocampal sharp-wave ripples feature spatial trajectories with momentum. *Neuron* **110**, 722–733 (2022).
- Maboudi, K., Giri, B., Miyawaki, H., Kemere, C. & Diba, K. Retuning of hippocampal representations during sleep. *Nature* **629**, 630–638 (2024).
- Csicsvari, J., Hirase, H., Mamiya, A. & Buzsaki, G. Ensemble patterns of hippocampal CA3-CA1 neurons during sharp wave-associated population events. *Neuron* **28**, 585–594 (2000).
- Tang, W., Shin, J. D., Frank, L. M. & Jadhav, S. P. Hippocampal-prefrontal reactivation during learning is stronger in awake compared with sleep states. *J. Neurosci.* **37**, 11789–11805 (2017).
- Tononi, G. & Cirelli, C. Sleep and the price of plasticity: from synaptic and cellular homeostasis to memory consolidation and integration. *Neuron* **81**, 12–34 (2014).
- Ponomarenko, A. A., Korotkova, T. M., Sergeeva, O. A. & Haas, H. L. Multiple GABAA receptor subtypes regulate hippocampal ripple oscillations. *Eur. J. Neurosci.* **20**, 2141–2148 (2004).
- Gordon, J. A., Lacefield, C. O., Kentros, C. G. & Hen, R. State-dependent alterations in hippocampal oscillations in serotonin 1A receptor-deficient mice. *J. Neurosci.* **25**, 6509–6519 (2005).
- Oliva, A., Fernandez-Ruiz, A., Buzsaki, G. & Berenyi, A. Role of hippocampal CA2 region in triggering sharp-wave ripples. *Neuron* **91**, 1342–1355 (2016).
- Nakashiba, T., Buhl, D. L., McHugh, T. J. & Tonegawa, S. Hippocampal CA3 output is crucial for ripple-associated reactivation and consolidation of memory. *Neuron* **62**, 781–787 (2009).
- Sebastian, E. R. et al. Topological analysis of sharp-wave ripple waveforms reveals input mechanisms behind feature variations. *Nat. Neurosci.* **26**, 2171–2181 (2023).
- Wiegand, J. P. et al. Age is associated with reduced sharp-wave ripple frequency and altered patterns of neuronal variability. *J. Neurosci.* **36**, 5650–5660 (2016).
- Ponomarenko, A. A., Li, J. S., Korotkova, T. M., Huston, J. P. & Haas, H. L. Frequency of network synchronization in the hippocampus marks learning. *Eur. J. Neurosci.* **27**, 3035–3042 (2008).
- Girardeau, G., Cei, A. & Zugaro, M. Learning-induced plasticity regulates hippocampal sharp wave-ripple drive. *J. Neurosci.* **34**, 5176–5183 (2014).
- Havekes, R. et al. Sleep deprivation causes memory deficits by negatively impacting neuronal connectivity in hippocampal area CA1. *eLife* **5**, e13424 (2016).
- Gerstner, J. R. et al. Removal of unwanted variation reveals novel patterns of gene expression linked to sleep homeostasis in murine cortex. *BMC Genomics* **17**, 727 (2016).

Publisher's note Springer Nature remains neutral with regard to jurisdictional claims in published maps and institutional affiliations.

Springer Nature or its licensor (e.g. a society or other partner) holds exclusive rights to this article under a publishing agreement with the author(s) or other rightsholder(s); author self-archiving of the accepted manuscript version of this article is solely governed by the terms of such publishing agreement and applicable law.

© The Author(s), under exclusive licence to Springer Nature Limited 2024

Methods

Animals and surgical procedures

Four male and three female Long-Evans rats (300–500 g, 10–15 weeks old) were used in this study. No sample size calculations were performed. The sample size was selected to adequately reflect the variability in reactivation during sleep deprivation. As one animal had a low number of stable units, an additional male rat was added. All surgeries were performed on isoflurane anaesthetized animals head fixed on a stereotaxic frame⁶¹. After removing hair from the head, the incision area was cleaned using alcohol and betadine. Next, an incision was made to expose the skull underneath. The skull was cleaned of tissues and blood, after which hydrogen peroxide was applied. Coordinates for probe implantation were marked above the dorsal hippocampus (anteroposterior, -3.36 ; mediolateral, ± 2.2) following measurement of bregma and lambda. Craniotomies were drilled at the marked location. Using a blunt needle, the dura was removed carefully to expose the brain surface. After cessation of bleeding, animals were implanted with 64-channel silicon probes (eight shanks Buzsaki; Neuronexus; one animal) or 128-channel silicon probes (eight shanks; Diagnostic Biochips; six animals). Ground and reference screws were placed over the cerebellum. Craniotomy was covered with DOWSIL silicone gel (3–4680, Dow Corning) and wax. A copper mesh was built around the implant for protection and electrical shielding. All procedures involving animals were approved by the Animal Care and Use Committee at the University of Michigan.

Behaviour

Before the probe implant surgery, animals were habituated to the experimenter for 40 min or more over 5 days. Following habituation, animals were water restricted and trained to associate water rewards with plastic wells. During the post-implant recovery period (7 days) animals were brought to the recording room for monitoring electrophysiology signals and probes were slowly lowered to the dorsal CA1 region of the hippocampus. In addition, animals were also habituated to sleep box for more than 1 h every day. Following this, animals were placed on a water restriction regiment for 24 h before experiments started. Each experimental session began by transferring animals to their sleep box about 4 h before the onset of light cycle. After 3 h of recording in the home cage, animals were transferred to a maze that they had not previously explored. These maze tracks were made distinct by the shape, colour and construction materials. Animals alternated for about 1 h between two water wells fixed at either end of the maze to retrieve rewards from water wells. Following exploration, animals were transferred to the home cage and the recording continued for 10 h or more in either SD or NSD, pseudo-randomly assigned. Owing to the unmistakable differences in the data across these groups, experimenters were not blinded to experimental conditions. Animals had access to ad libitum food and received ad libitum water for 30 min per day.

Sleep deprivation protocol

SD was performed at the onset of the light cycle in the home cage using a standard 'gentle handling' procedure^{62,63}. Animals were extensively habituated to the experimenter conducting the SD. During the initial hours of SD, animals were kept awake by mild noises, tapping or gentle shaking of the cage when they showed signs of sleepiness. As sleep pressure built up over a 5 h SD period, other techniques such as gently stroking the animal's body with a soft brush or disturbing bedding were increasingly used to ensure that they stayed awake. Following SD, animals were allowed to sleep and recover for 48 h before any further experiments.

Data acquisition

Electrophysiology data were acquired using OpenEphys⁶⁴ or an Intan RHD recording controller sampled at 30 kHz. Analysis of LFP was

performed on signals downsampled to 1,250 Hz. The animal's position on the maze track was obtained using Optitrack (NaturalPoint) hardware and Motive software (v.2.0, <https://optitrack.com/software/motive/>), which uses infrared cameras to locate markers clipped to the animal's crown. Three-dimensional position data were sampled at 60 or 120 Hz and later interpolated for aligning with electrophysiology. Water rewards during alternation on the maze track were delivered by means of solenoids interfaced with custom-built hardware using Arduino. The timestamps for water delivery were recorded by means of transistor–transistor logic pulses.

Spike sorting, cell classification and stability criteria

Raw data went through filtering, thresholding and automatic spike sorting using SpyKING CIRCUS (v.0.8.8–v.1.1.0, <https://github.com/spyking-circus/spyking-circus>)⁶⁵, followed by manual inspection and reclustering using the Phy package (v.2.0, <https://github.com/cortex-lab/phy/>). Only well-isolated units were used for further analysis with the exception of decoding/sequence detection analysis in which we used all clusters that satisfied the stability criteria.

LFP and unit analyses were performed using custom codes (NeuroPy) written in Python and are available in our laboratory's GitHub repository (v.0.1, <https://github.com/diba-lab/NeuroPy>) which uses the packages NumPy (v.1.24.4, <https://numpy.org>), SciPy (v.1.11.3, <https://scipy.org>) and pingouin (v.0.5.3, <https://pingouin-stats.org>) for data analysis and matplotlib (v.3.8.1, <https://matplotlib.org>) and Seaborn (v.0.11.2, <https://seaborn.pydata.org>) for visualization. Units were sorted into putative pyramidal cells and interneurons on the basis of peak waveform shape, firing rate and interspike interval^{66,67}.

With respect to stability criteria, to ensure that a given neuron was reliably tracked across the recording duration, we divided each session into five equally sized bins (about 2.5 h) and excluded any unit that fired below 25% of its overall mean in any given time bin.

Sharp-wave ripple detection and related properties

For detecting ripples, one channel from each shank was selected on the basis of the (highest) mean power in the ripple frequency band (125–250 Hz). The Hilbert amplitude was averaged across all selected channels, then smoothed using a Gaussian kernel ($\sigma = 12.5$ ms) and z-scored. Putative ripple epochs were identified from timepoints exceeding 2.5 s.d. and the start/stop was associated with signals of more than 0.5 s.d.; candidate ripples of more than 50 ms or more than 450 ms were excluded from further analyses. The maximum z-score value in a ripple epoch was termed as its ripple power. Sharp-wave amplitudes were obtained from a bandpass (2–30 Hz) filtered LFP using the difference between maximum and minimum value across all recorded channels in a given ripple. The peak frequency of each ripple was estimated using a complex wavelet transform. The LFP was first high-pass filtered at more than 100 Hz. This filtered signal was then convolved with complex Morlet wavelets with central frequencies selected from linearly spaced frequencies in the ripple frequency band (100–250 Hz). In each ripple, the frequency with maximum absolute wavelet power was designated as the peak ripple frequency.

Sleep scoring

Sleep scoring was performed using correlation electromyogram (EMG), theta and delta power. Correlation EMG was estimated by summing pairwise correlations across all channels calculated in 10 s time windows with a 1 s step^{68,69}. For theta power, a recording channel with the highest mean power in the 5–10 Hz theta frequency band was identified. Following theta channel selection, the power spectral density was calculated for each window. Periods with low and high EMG power were labelled as sleep and wake, respectively. The theta (5–10 Hz) over delta (1–4 Hz) plus (10–14 Hz) band ratio of the power spectral density was used to detect transitions between high theta and low theta, using custom python software based on hidden Markov models followed by visual

Article

inspection. Sleep states with high theta were classified as REM and the remainder were classified as NREM. Wake periods with high theta were labelled as 'active' and the remaining were labelled 'quiet'. These labels were merged in WAKE for the main figures. All detected states went through further visual inspection to correct any misclassifications. Detailed, interactive sleep scoring plots for each session are available at: https://github.com/diba-lab/sleep_loss_hippocampal_replay.

Detection of delta waves, delta power and OFF states

To detect hippocampal delta waves⁷⁰, hippocampal LFP was filtered (0.5–4 Hz) and the resulting filtered signal was z-scored. The first-order derivative of this signal was used to identify upward-downward-upward zero crossings, which corresponded to the beginning, peak and end of the delta wave, respectively. Delta waves lasting for less than 150 ms or more than 500 ms were discarded. In addition, we required the amplitude at peak to be either greater than 2 s.d. or the amplitude at peak more than 1 s.d. and amplitude at end less than -1.5 s.d.

Delta power spectral density was calculated by extracting LFP signal from a channel localized in the CA1 pyramidal cell layer with Welch's method using 4 s bins.

The multi-unit activity (MUA) smoothed with a Gaussian kernel of $\sigma = 20$ ms was used to detect OFF periods, following a method adapted from ref. 21. Candidate OFF periods were identified when the MUA firing rate dropped below the session median. The surrounding timepoints when the firing rate reached the lowest 10 percentile were used to mark the onset, offsets and corresponding duration of these events.

Explained variance measure for reactivation

Reactivation was assessed by the EV measure following previously described methods^{35,36}. This EV describes how much of the co-activity in a pair of neurons for a given window in POST is explained by the co-activity of those neurons during MAZE, while controlling for co-activity that was present during similar windows in PRE. Briefly, spike times were binned into 250 ms time bins, creating an N by T matrix, where N is the number of neurons and T is the number of time bins. Pearson's correlations, R , were determined for spike counts from neuronal pairs in 15 min sliding windows (window length 15 min, sliding 5 min steps) to produce \mathbf{P} , an M -dimensional vector, where M is the number of cell pairs. To reduce spurious correlations arising from cross contamination of units from the same shank⁷¹, only pairs with waveform similarity of less than 0.8 were used. Next, to assess similarity between \mathbf{P} vectors from different windows, the Pearson correlation R of these vectors (that is, the correlation between cell pair correlations) was determined (for example, $R_{[\text{PRE}, \text{POST}]}$, $R_{[\text{PRE}, \text{MAZE}]}$ and $R_{[\text{MAZE}, \text{POST}]}$). Controlling for pre-existing correlations in a given sliding window (k) in PRE, the EV for a 15 min window (WIN) was calculated as:

$$\text{EV}(\text{WIN}) = \left(\frac{R_{[\text{MAZE}, \text{WIN}]} - R_{[\text{MAZE}, \text{PRE}(k)]} \times R_{[\text{PRE}(k), \text{WIN}]} }{\sqrt{1 - R_{[\text{MAZE}, \text{PRE}(k)]}^2} \sqrt{1 - R_{[\text{PRE}(k), \text{WIN}]}^2}} \right)^2$$

averaged over all windows in PRE. To get an estimate of the chance level for EV, we calculated REV for each WIN^{37,72}:

$$\text{REV}(\text{WIN}) = \left(\frac{R_{[\text{MAZE}, \text{PRE}(k)]} - R_{[\text{MAZE}, \text{WIN}]} \times R_{[\text{PRE}(k), \text{WIN}]} }{\sqrt{1 - R_{[\text{MAZE}, \text{PRE}(k)]}^2} \sqrt{1 - R_{[\text{PRE}(k), \text{WIN}]}^2}} \right)^2$$

similarly averaged over PRE.

To estimate the time constant of reactivation from each session³⁵, we fit the time course, t , of bootstrap and session EV curves to an exponential function:

$$\text{EV}(t) = ae^{-t/\tau}$$

where τ provides the exponential decay constant and a is a scaling factor.

Only sessions with more than 15 stable units were used in the reactivation and replay analyses (13 of 16 recorded sessions from six of seven animals).

Place field calculations

To calculate one-dimensional place fields, animals' two-dimensional positions were linearized using ISOMAP⁷³ and visually inspected to ensure accuracy. For each unit, two firing-rate maps were generated corresponding to each running direction. Occupancy within 2 cm spatial bins at timepoints when the animal's speed exceeded 8 cm s^{-1} were calculated and smoothed with a Gaussian kernel ($\sigma = 4 \text{ cm}$). For each neuron, spike counts in each spatial bin were determined and also smoothed with the Gaussian kernel ($\sigma = 4 \text{ cm}$). Then, each neuron's firing-rate map was generated by dividing the smoothed spike counts by the smoothed occupancy map. Neurons with peak firing rate of less than 0.5 Hz were excluded from further analysis.

Decoding and trajectory replays

MUA was used to detect population burst events that are concurrent with SWR. In a session, the firing rate of MUA was derived from all putative spikes combined from all clusters then binned in 1 ms time bin and smoothed using a Gaussian kernel of $\sigma = 20$ ms. Periods with peak MUA > 3 s.d. above the mean firing rate were considered candidate ripple events. The start and end times of these ripple events were defined by the first neighbouring timepoints at which the MUA exceeded the mean. Ripple events occurring within 10 ms of each other were merged. Ripple events with duration of less than 80 ms or greater than 500 ms were discarded.

Before decoding, candidate ripple events were required to satisfy (1) five or more active units, (2) movement speed of less than 8 cm s^{-1} and (3) concurrent peak ripple power of more than 1 s.d. For these analyses alone, to minimize decoding error, we included all stable clusters with a mean firing rate of less than 10 Hz, regardless of their isolation quality⁷⁴. Position decoding was carried out on ripple events using standard Bayesian decoding⁷⁵ methods. Probabilities of the animal occupying each position bin x_p on the track were calculated according to:

$$P(x_p | n_t) = K_t \left\{ \prod_{i=1}^N \lambda_i[x_p]^{n_{i,t}} \right\} e^{-\tau \sum_{i=1}^N \lambda_i[x_p]}$$

where τ is the duration of the time bin (20 ms) used, $\lambda_i[x_p]$ is the firing rate of the i th neuron at x_p on the maze, K_t is a normalization constant to ensure that the sum of probabilities across all position bins equals to 1 and $n_{i,t}$ is the number of spikes fired by each neuron in that bin. The location with the maximum posterior probability was considered the 'decoded location' for each time bin. A candidate ripple event was classified as a 'trajectory replay' if it decoded a continuous trajectory across space for 60 ms or more, such that the distance between decoded locations in adjacent time bins was less than 40 cm. Posterior probability matrices for all ripple events that were classified as replay have been compiled in an interactive plot available in our GitHub repository (https://github.com/diba-lab/sleep_loss_hippocampal_replay).

Hierarchical bootstrapping

We used HB²⁶ to estimate confidence intervals and P values for different variables following code found at <https://github.com/soberlab/Hierarchical-Bootstrap-Paper>. For each metric we generated a population of 10,000 values by resampling with replacement at each level of the data hierarchy (first sessions, then for each session, the variable measured; for example, frequency of the SWR) and pooled the values to calculate the test statistic and corresponding confidence interval or IQR. Two-tailed tests with $\alpha = 0.05$ were used for within-group

comparisons, in which the P value was determined from the proportion of bootstraps for which the test statistic in one group exceeded that of the other group. The within-group comparisons generated one-sided hypotheses for cross-group testing, performed at $\alpha = 0.05$. For these cross-group comparisons, we used the joint probability distributions of the bootstrapped samples to determine the P value: the likelihood that the mean of group one is greater than or equal to the mean of group two. All HB data were visualized using box and whisker plots generated using the boxplot function from the matplotlib (v.3.8.1) and Seaborn (v.0.11.2) Python packages to depict the median and first or third quartiles, with whiskers extending to $1.5 \times$ IQR. For testing if firing-rate distributions differed from log-normal, Shapiro–Wilk tests were performed on each bootstrapped log distribution and the P value was determined from the proportion of bootstraps with significant skew at $\alpha = 0.05$. Detailed statistics with estimated P values for all performed comparisons are found in the Supplementary Table 1.

Parametric statistics

For instances in which parametric tests were more appropriate, the exact P values, test statistics, confidence intervals and degrees of freedom are provided in the Supplementary Table 2.

Reporting summary

Further information on research design is available in the Nature Portfolio Reporting Summary linked to this article.

Data availability

The processed group data for this study are available at <https://doi.org/10.7302/73hn-m920>, which includes NumPy (.npz) files used to generate most of the figures in this study. The remainder of the long-duration datasets generated during and analysed for the present study will be made available by the corresponding author on request.

Code availability

All analyses were performed using custom codes written in Python. General-purpose code is available in our laboratory's public GitHub repository (<https://github.com/diba-lab/NeuroPy>, v.0.1). Code specific to this project and used for generating figures herein is located at https://github.com/diba-lab/sleep_loss_hippocampal_replay (v.0.2).

61. Kinsky, N. R. et al. Simultaneous electrophysiology and optogenetic perturbation of the same neurons in chronically implanted animals using μ LED silicon probes. *STAR Protoc.* **4**, 102570 (2023).
62. Colavito, V. et al. Experimental sleep deprivation as a tool to test memory deficits in rodents. *Front. Syst. Neurosci.* **7**, 106 (2013).
63. Prince, T. M. et al. Sleep deprivation during a specific 3-hour time window post-training impairs hippocampal synaptic plasticity and memory. *Neurobiol. Learn. Mem.* **109**, 122–130 (2014).
64. Siegle, J. H. et al. Open Ephys: an open-source, plugin-based platform for multichannel electrophysiology. *J. Neural Eng.* **14**, 045003 (2017).
65. Yger, P. et al. A spike sorting toolbox for up to thousands of electrodes validated with ground truth recordings in vitro and in vivo. *eLife* **7**, e34518 (2018).
66. Petersen, P. C., Siegle, J. H., Steinmetz, N. A., Mahallati, S. & Buzsáki, G. CellExplorer: a framework for visualizing and characterizing single neurons. *Neuron* **109**, 3594–3608 (2021).
67. Bartho, P. et al. Characterization of neocortical principal cells and interneurons by network interactions and extracellular features. *J. Neurophysiol.* **92**, 600–608 (2004).
68. Schomburg, E. W. et al. Theta phase segregation of input-specific gamma patterns in entorhinal-hippocampal networks. *Neuron* **84**, 470–485 (2014).
69. Miyawaki, H., Billeh, Y. N. & Diba, K. Low activity microstates during sleep. *Sleep* **40**, zsx066 (2017).
70. Maingret, N., Girardeau, G., Todorova, R., Goutier, M. & Zugaro, M. Hippocampo-cortical coupling mediates memory consolidation during sleep. *Nat. Neurosci.* **19**, 959–964 (2016).
71. Quirk, M. C. & Wilson, M. A. Interaction between spike waveform classification and temporal sequence detection. *J. Neurosci. Methods* **94**, 41–52 (1999).
72. Tatsuno, M., Lipa, P. & McNaughton, B. L. Methodological considerations on the use of template matching to study long-lasting memory trace replay. *J. Neurosci.* **26**, 10727–10742 (2006).
73. Tenenbaum, J. B., de Silva, V. & Langford, J. C. A global geometric framework for nonlinear dimensionality reduction. *Science* **290**, 2319–2323 (2000).
74. van der Meer, M. A. A., Carey, A. A. & Tanaka, Y. Optimizing for generalization in the decoding of internally generated activity in the hippocampus. *Hippocampus* **27**, 580–595 (2017).
75. Davidson, T. J., Kloosterman, F. & Wilson, M. A. Hippocampal replay of extended experience. *Neuron* **63**, 497–507 (2009).
76. Marmelshtein, A., Eckerling, A., Hadad, B., Ben-Eliyahu, S. & Nir, Y. Sleep-like changes in neural processing emerge during sleep deprivation in early auditory cortex. *Curr. Biol.* **33**, 2925–2940 (2023).

Acknowledgements This work was funded by the US National Institute of Mental Health (R01MH117964 to K.D. and T.A.) and by the US National Institute of Neurological Disorders and Stroke (R01NS115233 to K.D.).

Author contributions K.D., T.A. and B.G. conceived the project. B.G. performed the experiments. B.G. and N.K. analysed the data. U.K. and K.M. contributed analytical insights. K.D. supervised the research. K.D. and B.G. wrote the manuscript with input and edits from T.A. and N.K.

Competing interests The authors declare no competing interests.

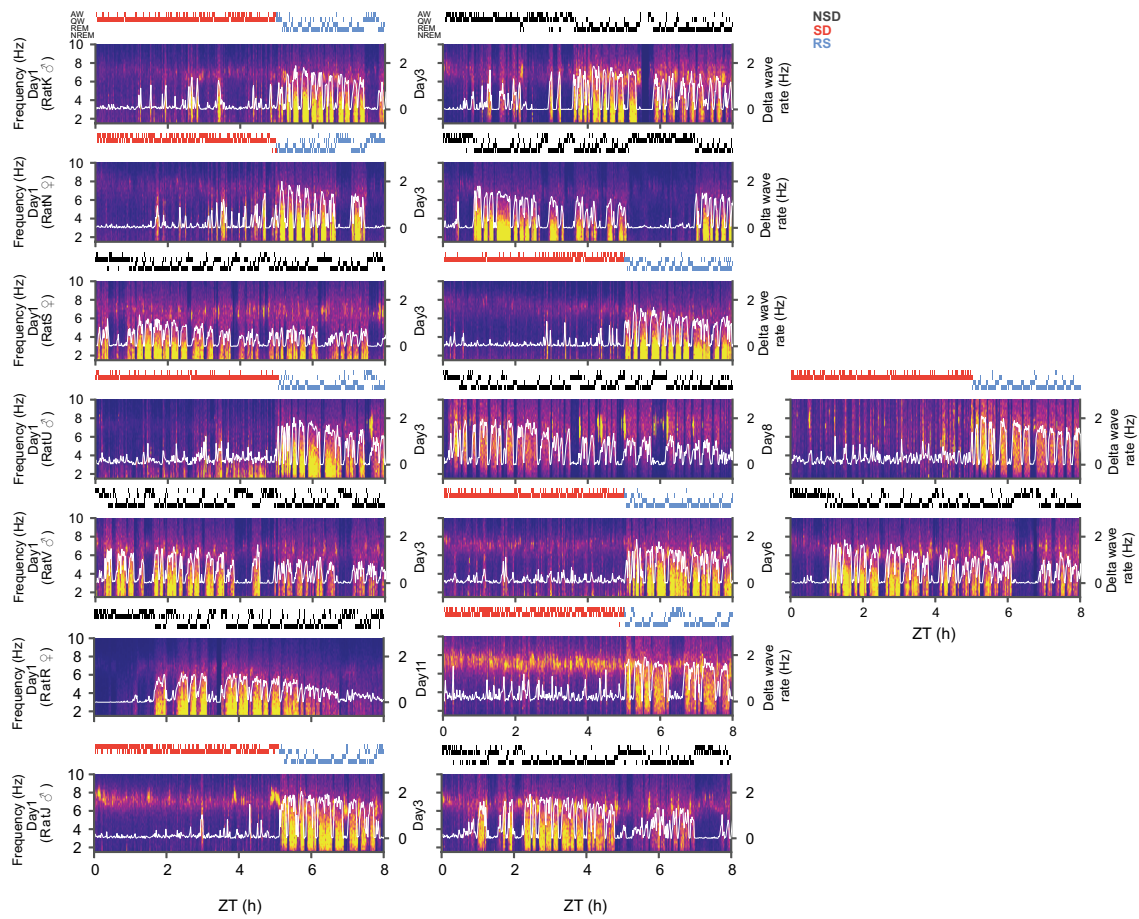
Additional information

Supplementary information The online version contains supplementary material available at <https://doi.org/10.1038/s41586-024-07538-2>.

Correspondence and requests for materials should be addressed to Kamran Diba.

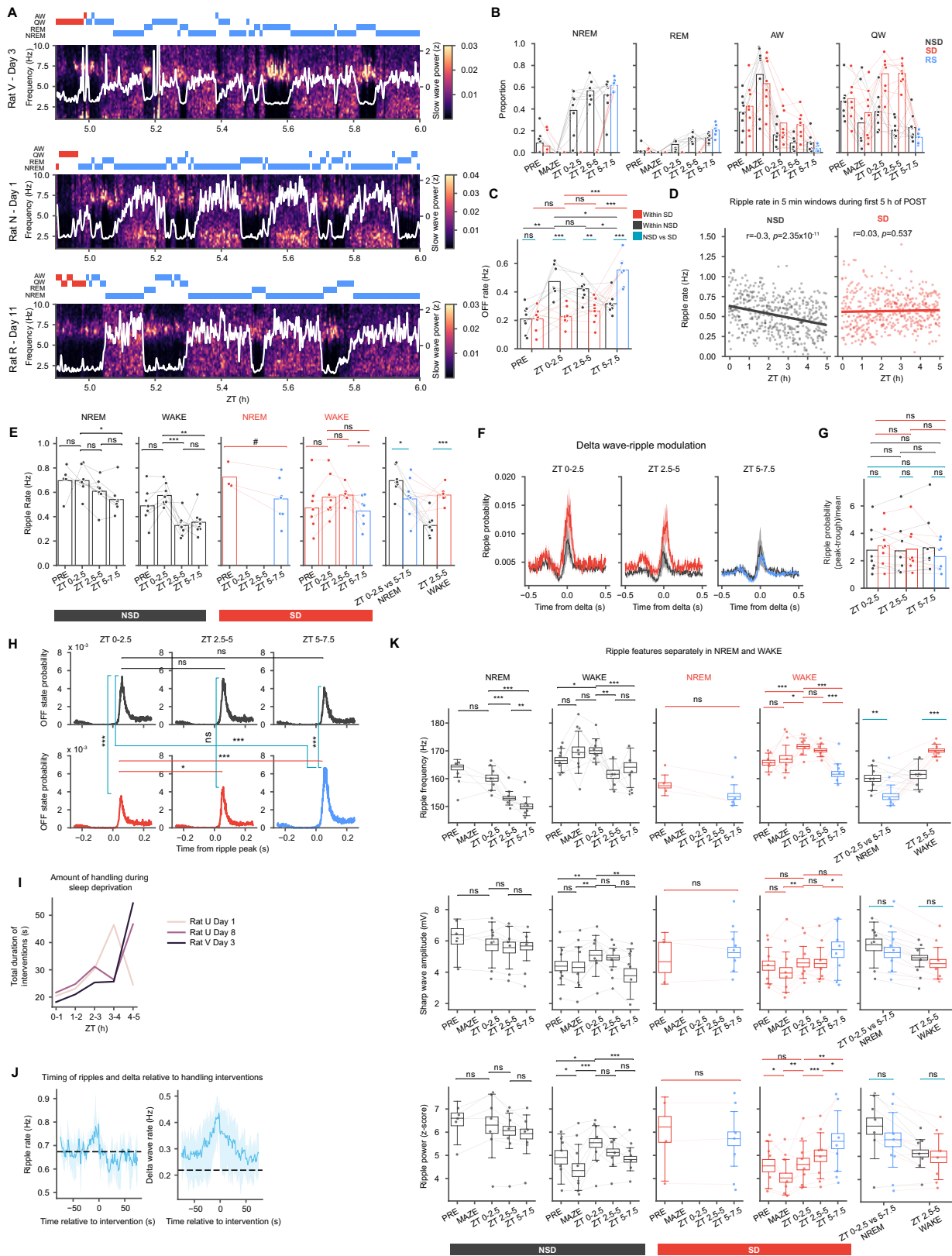
Peer review information Nature thanks Antoine Adamantidis, Vladyslav Vyazovskiy and the other, anonymous, reviewer(s) for their contribution to the peer review of this work. Peer reviewer reports are available.

Reprints and permissions information is available at <http://www.nature.com/reprints>.



Extended Data Fig. 1 | Power spectra and delta for all recorded sessions. Power spectral density of the CA1 local field potential (LFP), z-scored over 1–10 Hz for the time periods shown, with temporal evolution of delta (white) overlaid for each recorded session (similar to in Fig. 1b). Hypnograms above each panel show the brain state (active wake (AW), quiet wake (QW), rapid-eye

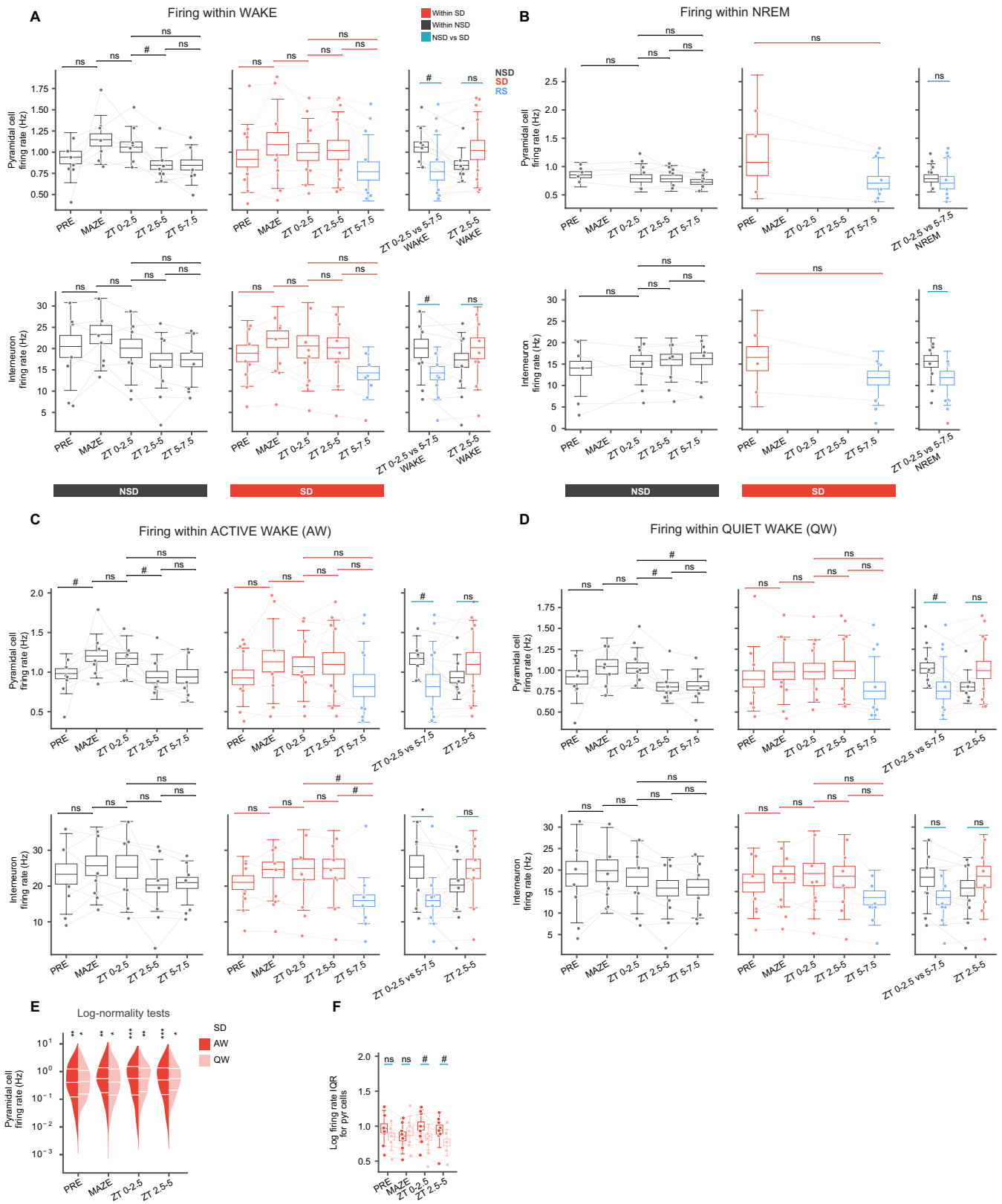
movement (REM) sleep and non-REM sleep (NREM)). State scoring was performed at 1-s resolution but for illustration purposes is provided averaged for 30-s periods (particularly due to rapid transitions between AW and QW during SD). Animal name initial, sex and recording day are provided the left of the y-axes.



Extended Data Fig. 2 | See next page for caption.

Extended Data Fig. 2 | Ripple and delta features and controls across sleep and sleep deprivation sessions. (A) Local field potential spectrogram (1–10 Hz) from a sample theta channel during recovery sleep (RS) from three rats with corresponding hypnogram indicating the scored sleep/wake state above (active wake (AW), quiet wake (QW), rapid eye movement (REM) and non-REM (NREM) sleep). The Fourier spectrogram was calculated from the whitened LFP traces using 4 s windows with 1 s overlap. Z-scored delta power (1–4 Hz, smoothed with a 12 s gaussian kernel) is overlaid in white. More detailed sleep scored sessions are available at https://github.com/diba-lab/sleep_loss_hippocampal_replay. (B) The proportion of time spent in each brain state across all sessions. Individual session values overlaid in connected dots ($n = 8$ NSD session and $n = 8$ SD sessions). We note that during sleep deprivation from ZT 0-2.5 (SD1) to ZT 2.5-5 (SD2), there was no significant change in the proportion of time in QW ($P = 0.958$, $t(df = 7) = -0.054$) or AW ($P = 0.769$, $t(df = 7) = 0.305$). (C) The rate of OFF states compared across sessions. For the non-sleep-deprived (NSD) group, OFF states were most prevalent during NS1 (ZT 0-2.5) and decreased over time, in NS2 (ZT 2.5-5) and NS3 (ZT 5-7.5). The rate of OFF states was initially lower in the SD group, but increased from SD1 to SD2, with a further large increase upon RS. (D) The rate of ripple events calculated in 5 min windows decreased over the first 5 h of NSD but remained stable during 5 h of SD. (E) Ripple rate calculated separately for NREM and WAKE states (individual sessions overlaid with connected dots). A decrease in ripple rates is observed in both NREM and WAKE in the NSD group, but there was no change in WAKE ripples from SD1 to SD2 and a decrease from SD2 to RS. Overall, NREM ripple rates were higher in NS1 vs. RS and WAKE ripple rates were higher in SD2 vs. NS2. (F) The ripple probability (solid line = mean, shaded region = s.e.m., $n = 8$) was modulated by delta waves. (G) However, the modulation depth of ripples by delta ((peak-trough)/mean) was not significantly different across 2.5 h blocks. (H) OFF states were frequently preceded and followed by ripples⁶⁹. Modulation of OFF states by ripples did not change across NSD ($n = 103,319$ ripples across

8 sessions) but the probability that OFF immediately followed a ripple increased over SD, from SD1 to SD2 and further in RS, with a significant difference between RS and NS1. The inducement of OFF states by ripples is similar to the rise in OFF states following bursts induced by sensory stimulation in the cortex⁷⁶. (I) Interventions needed to stop transitions to sleep during SD were tracked using piezo sensors on the sides of the home cage in 3 sessions. The number of interventions grew with time during SD. (J) Mean and 95% confidence intervals of ripple rate (left) and delta wave rate (right) relative to the onset of interventions. The rate of delta waves and concurrent ripples was higher immediately preceding interventions, consistent with signs of sleepiness that compel such interventions. (K) Ripple features (frequency, sharp wave amplitude and ripple power) evaluated separately in NREM ($n = 67007$ ripples from 6 NSD sessions, $n = 26798$ ripples from 7 SD sessions) and WAKE states ($n = 74363$ ripples from 6 NSD sessions and 128957 ripples from 7 SD sessions). Rightmost panels in each row provide cross-group comparisons in NS1 vs. RS strictly during NREM and NS2 vs. SD2 strictly during WAKE. These results are largely consistent with patterns in Fig. 1g–i, except that here ripple power in NS2 vs. SD2 is not significantly different during WAKE, indicating state-dependence of this effect. Additionally, we note a significant increase in ripple frequency in WAKE from PRE to POST in both NSD and SD groups, indicating an effect of the novel maze exposure. All box plots show the median and top/bottom quartiles (whiskers = 1.5 x interquartile range) of the hierarchically bootstrapped data with individual session means overlaid with connecting dots. Statistics: panels C, E, G, two-sided paired t-tests (within group) and one-sided independent groups (across groups) t-tests; panel D, Pearson correlation coefficients with two-sided p-value; panel H, χ^2 tests of independence; panel K, two-sided paired within group and one-sided cross-group comparisons with hierarchical bootstrapping; ns (not significant), * $P < 0.05$, ** $P < 0.01$, *** $P < 0.001$, with no correction for multiple comparisons. See Supplementary Tables 1 and 2 for additional details.



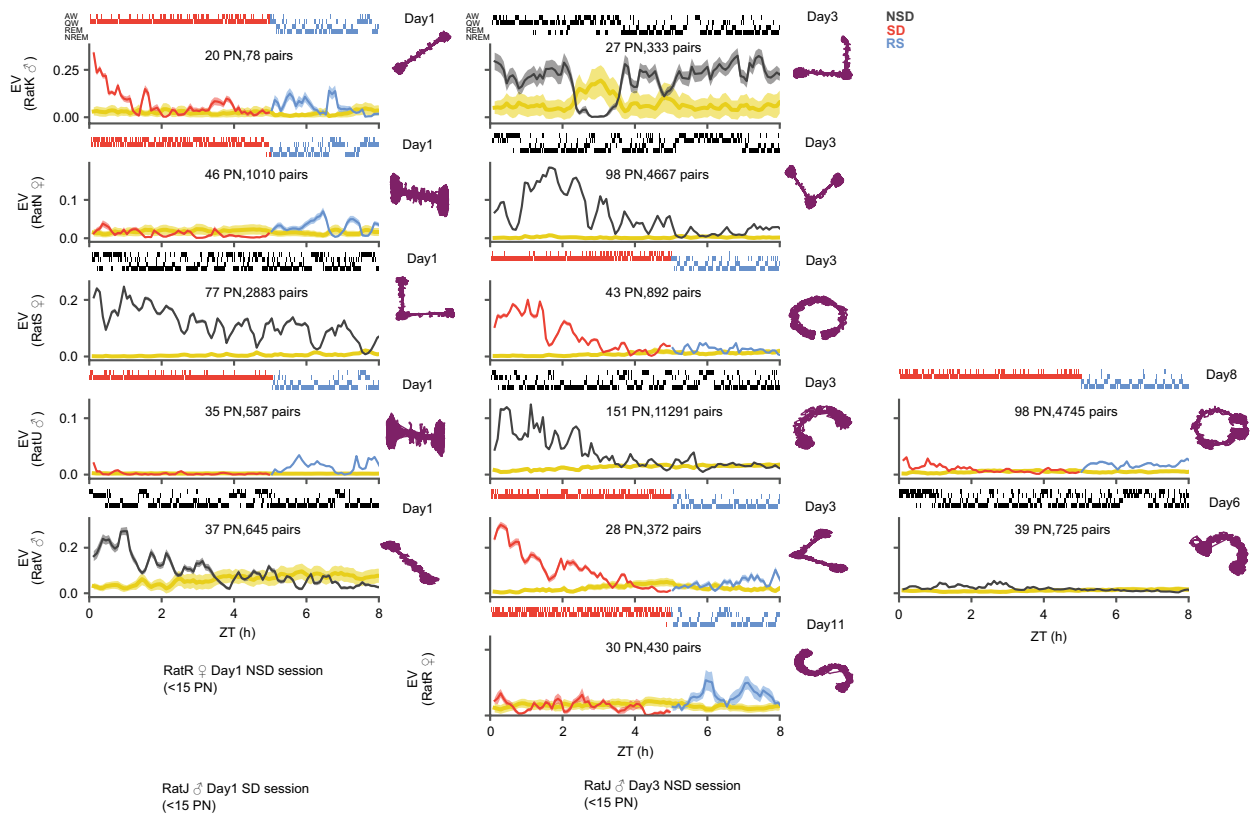
Extended Data Fig. 3 | See next page for caption.

Article

Extended Data Fig. 3 | Firing rate changes within each state separately.

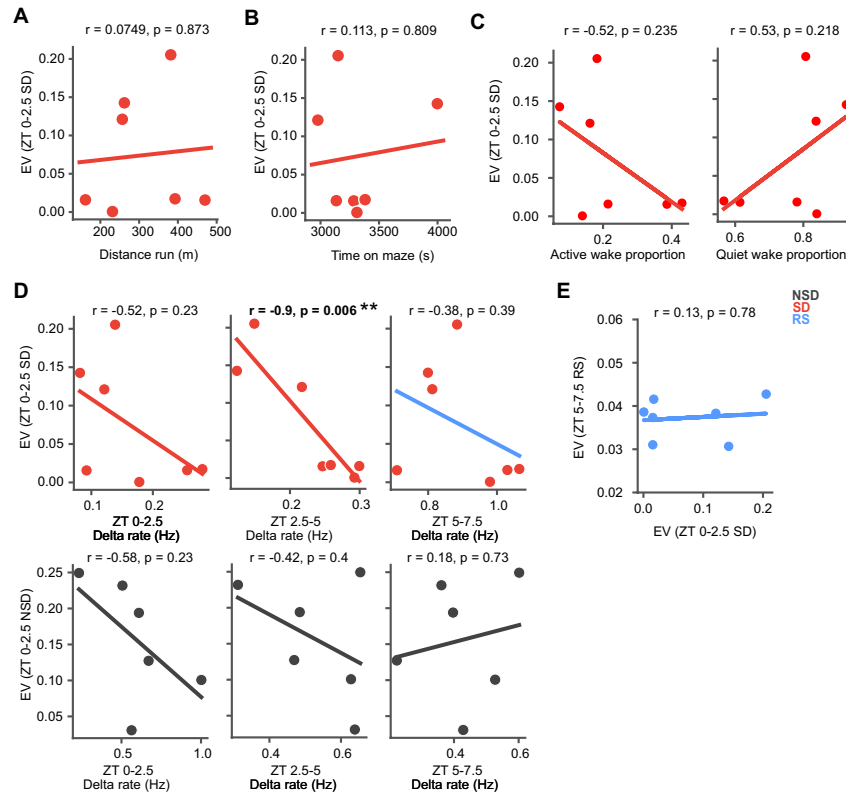
Mean firing rates calculated solely within the awake (WAKE) state (A) or solely within NREM (B) with individual sessions overlaid and connected. Differences calculated separately within wake or NREM were less pronounced than those shown in Fig. 2b,c, consistent with the noted effect of background state on hippocampal firing rates^{25,29}. However, when estimating the metabolic cost of neuronal firing²³, comparisons that overlook the state and consider temporal variations in rates, such as those depicted in Fig. 2b and c, are most appropriate. In WAKE (A), firing rates showed a trend towards decreased rates in pyramidal cells (top row) in the NSD group ($n = 442$ neurons from 8 sessions) but not in SD ($n = 312$ neurons from 8 sessions). The decrease in firing rates during brief wakings with the recovery sleep period (right panel) likewise showed a trend towards significance vs. a similar period in NSD. Interneuron firing rates (bottom row) within WAKE in recovery sleep showed a trend towards significance in comparison to the similar period in NSD ($n = 48$ cells from 8 NSD

sessions and $n = 48$ cells from 8 SD sessions). In NREM (B) no significant differences were detected across groups or periods. (C) and (D) Same as (A) and (B) but for active wake (AW) and quiet wake (QW). (E) Firing rate distribution for all pyramidal cells recorded during SD sessions for AW vs. QW. Firing rates in both WAKE states remain skewed from log-normal distribution throughout SD. (F) Interquartile range (IQR) of the log firing rate of pyramidal cells reveals a trend toward a broader range of firing rates in AW vs. QW during SD. All box plots depict the median and top/bottom quartiles (whiskers = 1.5 x interquartile range) of the hierarchically bootstrapped data with individual session means overlaid with connecting dots. Statistics: A-D, F: two-sided paired within group and one-sided cross-group comparisons with hierarchical bootstrapping; E: Shapiro-Wilk tests performed on each bootstrapped log distribution, with P obtained from the proportion of bootstraps with significant skew; ns (not significant), # $P < 0.1$, * $P < 0.05$, ** $P < 0.01$, *** $P < 0.001$, with no correction for multiple comparisons. See Supplementary Table 1 for additional details.



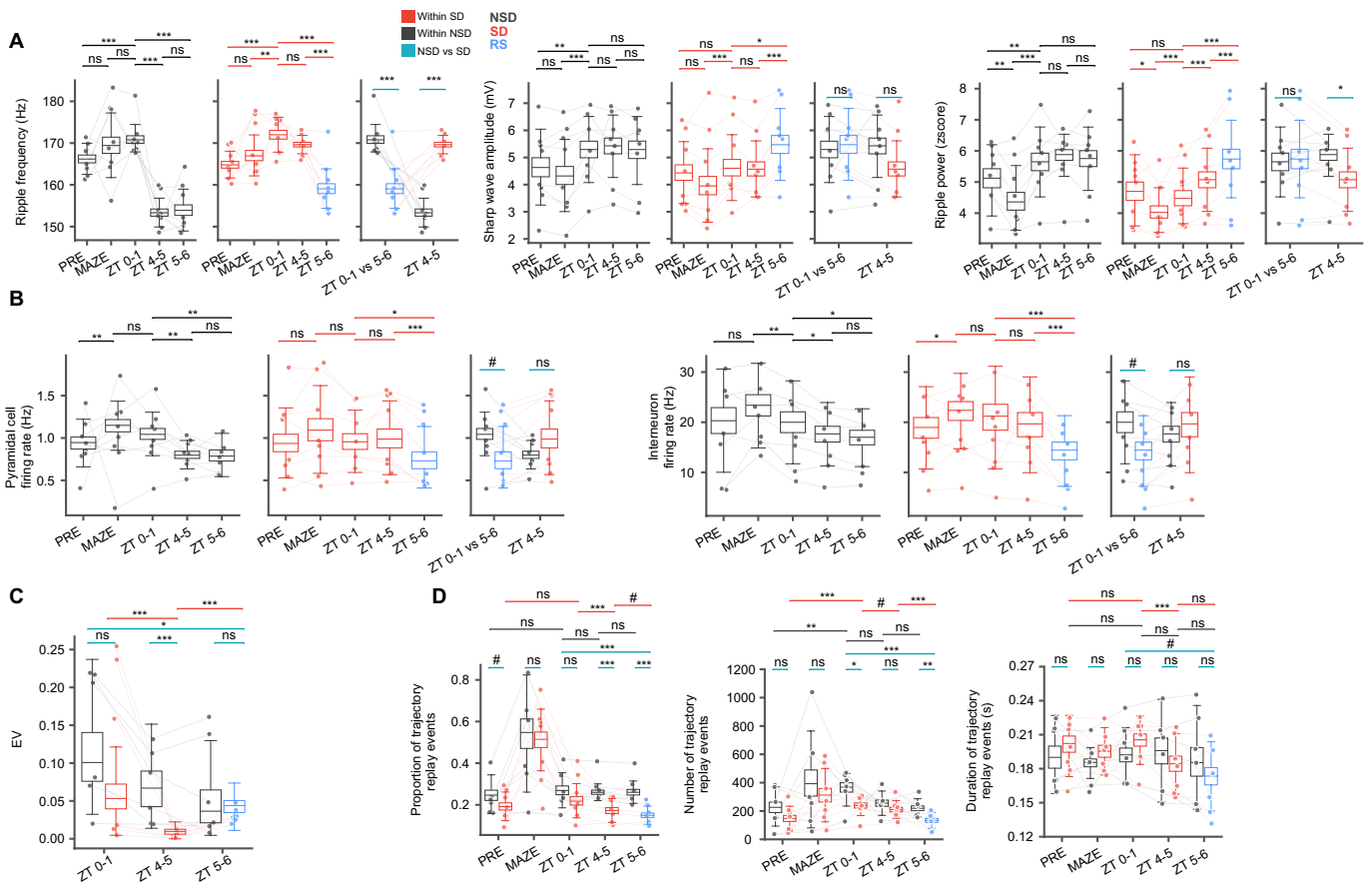
Extended Data Fig. 4 | Temporal evolution of reactivation across recorded sessions. Reactivation assessed using the explained variance (EV) metric (NSD (black), SD (red) and RS (blue)), in thirteen sessions from six different animals (3 male and 3 female, with 3 sessions from 2 animals (1 male, 1 female) excluded due to an insufficient number of stable neurons), as in Fig. 3a. Chance level (REV) is shown in maize. Solid lines show the mean and shaded regions show the standard deviation of EV/REV across all 15 min windows in POST. Each row

provides session(s) from one animal, with number of putative pyramidal neurons and cell pairs used to calculate EV specified inside each panel. Hypnograms above panels depict sleep/wake history in active wake (AW), quiet wake (QW), rapid eye movement (REM) sleep and non-REM (NREM) sleep, with sleep deprivation/recovery sleep in red/blue and natural sleep in black. Animals' tracked positions on the novel maze (purple) are depicted on the right of the panels along with the session recording day.



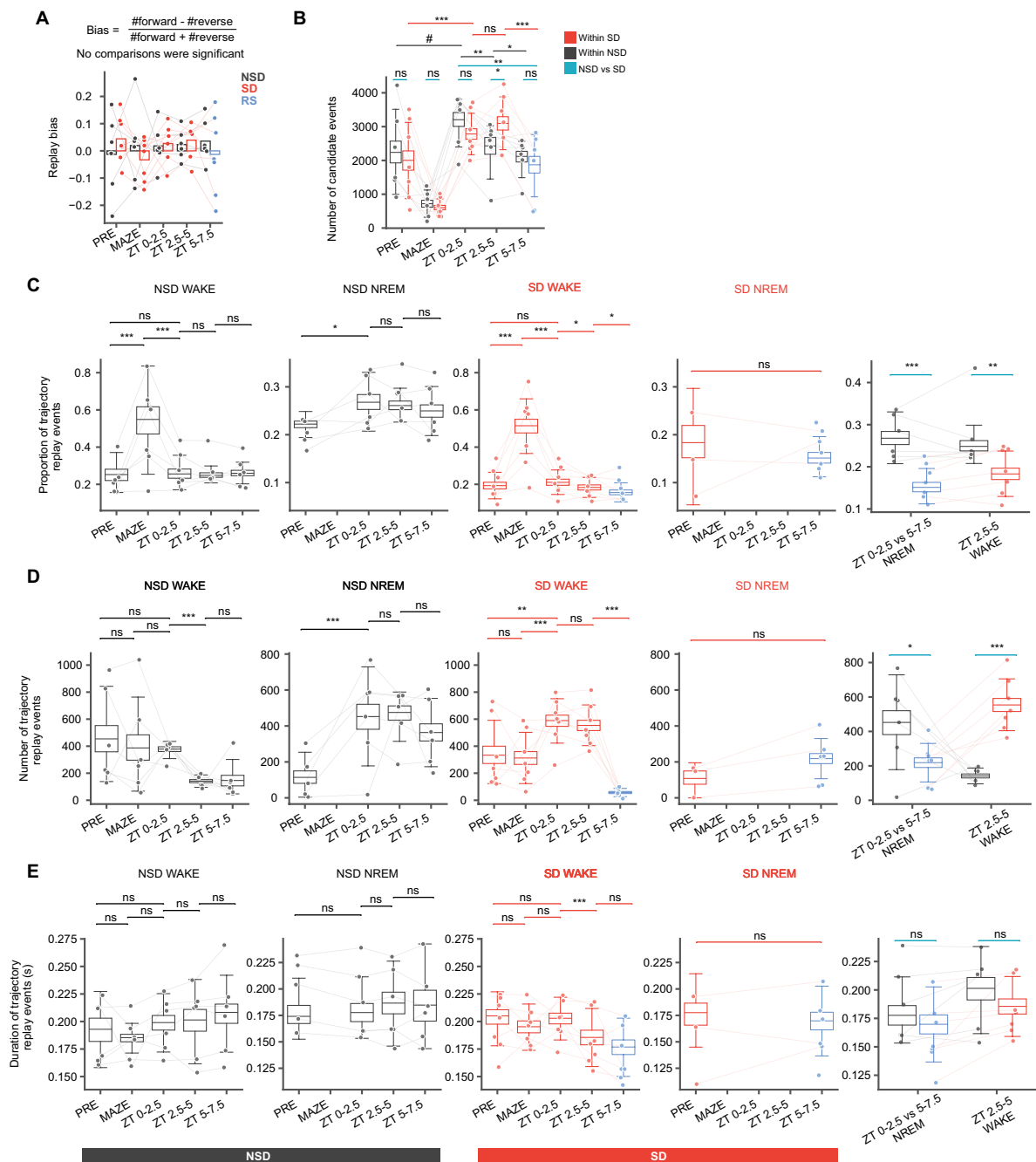
Extended Data Fig. 5 | Accounting for the variability in reactivation during sleep deprivation. We observed striking variability in reactivation across animals during the first block of sleep deprivation (SD1) in ZT0-2.5 (Fig. 3 and Extended Data Fig. 4). We conducted a series of analyses in an effort to account for this observation. Differences in (A) the distance run or (B) the total time spent running on the maze, did not account for the variance in EV during SD1. (C) Likewise, the variance in EV during SD1 cannot be attributed to differences in the proportion of time in active wake (left) or quiet wake (right) states during this period. (D) We next tested whether the rate of delta waves during sleep deprivation (top row, $n = 7$ sessions), an indicator of sleep pressure, could explain the variance in EV during SD1. Remarkably, there was a strong

significant negative correlation ($P = 0.006$) between the rate of delta from ZT 2.5-5 (SD2) and the reactivation (EV) during SD1. If delta during SD2 thus relates to animal's level sleepiness, consistent with the sleep homeostasis model^{24,38}, the level of sleepiness correlates with the amount of hippocampal reactivation we observe during SD1. In contrast, we observed no correlation between EV and delta at any timepoint for NSD (bottom row, $n = 6$ sessions). (E) A similar relationship was not evident between delta waves and EV in NS2. (F) Reactivation (EV) during SD1 was not predictive of the reactivation during RS. Statistics: All panels, Pearson correlation coefficients with two-sided P -values, $**P < 0.01$, with no correction for multiple comparisons.



Extended Data Fig. 6 | Comparisons across 1-hour blocks. Changes in ripple properties, firing rates, explained variance and replays were assessed using 1-h blocks, based on the last hour of PRE, 1-h periods immediately after MAZE (ZT 0-1) and 1-h blocks immediately before and after recovery sleep (ZT 4-5 and ZT 5-6). All box plots depict the median and top/bottom quartiles (whiskers = 1.5 x interquartile range) of the hierarchically bootstrapped data with individual session means overlaid with connecting dots. Similar to our results for 2.5 h blocks in the main text, **(A)** ripple frequency (left) decreased over NSD ($n = 143681$ ripples total from 8 sessions) but increased in SD ($n = 157964$ ripples total from 8 sessions) relative to MAZE, with a rebound drop in RS (ZT 5-6). Rightmost panel highlights cross-group comparisons for the first block of sleep (NS1 vs. RS) and second block of SD vs. NSD. In both groups, sharp-wave amplitudes (middle) and ripple power (right) increased from MAZE to the first block of POST (ZT 0-1). Sharp-wave amplitude (middle) and ripple power (right) further increased in RS. Cross-group comparisons at ZT 4-5 showed increased ripple power in NSD compared to SD. **(B)** Firing rate of pyramidal neurons show decreasing firing rates during sleep but not during SD ($n = 442$ pyramidal

neurons / 48 interneurons from 8 sessions NSD, 312 pyramidal neurons / 48 interneurons from 8 sessions SD). **(C)** EV was significantly lower in SD at ZT4-5 compared to NSD, with a modest but significant rebound during RS, but to lower levels than during the first hour of natural sleep. $n = 20544$ cell-pairs from 6 NSD sessions and $n = 8114$ cell-pairs from 7 SD sessions. **(D)** The proportion of candidate ripple events that decoded continuous trajectories in different epochs ($n = 65744$ candidate events from 7 SD sessions and $n = 56669$ candidate events from 6 NSD sessions). SD sessions featured significantly fewer trajectory replays by ZT4-5. Critically, the proportion of replays in RS was significantly lower than in NS1. Similar results were observed for replay number (middle). A significant decrease was observed in mean replay event duration (right) for SD ($n = 13911$ replays from 7 sessions) but not NSD ($n = 15866$ replays from 6 sessions) from ZT0-1 to ZT4-5. Statistics: two-sided within-group comparisons and one-sided cross-group comparisons with hierarchical bootstrap, $\#P < 0.1$, $*P < 0.05$, $**P < 0.01$, $***P < 0.001$, with no correction for multiple comparisons. See Supplementary Table 1 for additional details.



Extended Data Fig. 7 | Replay characterization during NREM and WAKE.

(A) Replays showed no bias in directionality. (B) The total number of candidate events decreased during POST in non sleep-deprivation (NSD, $n = 64205$ candidate events from 6 sessions) but remained elevated during sleep deprivation (SD, $n = 72584$ candidate events from 7 sessions) from the first to second block (SD1 to SD2), but dropping from SD2 to recovery sleep (RS). (C) The proportion of candidate events that scored as trajectory replays in NSD and SD groups, measured separately in WAKE ($n = 30852$ events from 6 NSD sessions and $n = 59820$ events from 7 SD sessions) and NREM ($n = 32258$ events from 6 NSD sessions and 11903 events from 7 SD sessions) states in each block. The rightmost panel compares between the first block of extended NREM sleep for each group (ZT 0-2.5 in the NSD group vs. ZT 5-7.5 in the SD group) and between WAKE during the second (late) block of POST (ZT 2.5-5 for both groups). There was a significantly lower proportion of trajectory replays in NREM recovery sleep (RS) compared to natural sleep (NS1) and fewer in WAKE (SD2 vs. NS2), demonstrating that these results were significant when assessed within states as well as when compared across time blocks that involved pooled states, as in Fig. 4. Note also that there was a significant increase in the proportion of trajectory replays during NREM from PRE to

POST, consistent with previous studies indicating increased replay following novel MAZE exposure^{43,44}. (D) Same as (C) but for the total number of trajectory replay events. Interestingly, the total number of trajectory replays decreased within WAKE in the NSD group, but did not change within SD, resulting in a greater total number of trajectory replays in SD2 compared to NS2. Importantly, however, there were significantly fewer trajectory replays in NREM RS vs. NS1. (E) Same as (C) but for duration of trajectory replay events (NREM: $n = 8291$ replays from 6 NSD sessions, $n = 1869$ replays from 7 SD sessions; WAKE: $n = 9128$ replays from 6 NSD sessions, $n = 12940$ replays from 7 NSD sessions). Note the decreased duration of these events during waking in SD2 vs. SD1. All box plots depict the median and top/bottom quartiles (whiskers = 1.5 x interquartile range) of the hierarchically bootstrapped data with individual session means overlaid with connecting dots. Statistics: Panel A: two-tailed, paired t-tests for within group comparisons and one-tailed Welch's t-tests for cross-group comparisons; Panels B-E, two-sided within-group comparisons and one-sided cross-group comparisons with hierarchical bootstrap, $^{\#}P < 0.01$, $^{*}P < 0.05$, $^{**}P < 0.01$, $^{***}P < 0.001$, with no correction for multiple comparisons. See Supplementary Tables 1 and 2 for additional details.

Reporting Summary

Nature Portfolio wishes to improve the reproducibility of the work that we publish. This form provides structure for consistency and transparency in reporting. For further information on Nature Portfolio policies, see our [Editorial Policies](#) and the [Editorial Policy Checklist](#).

Statistics

For all statistical analyses, confirm that the following items are present in the figure legend, table legend, main text, or Methods section.

n/a Confirmed

- The exact sample size (n) for each experimental group/condition, given as a discrete number and unit of measurement
- A statement on whether measurements were taken from distinct samples or whether the same sample was measured repeatedly
- The statistical test(s) used AND whether they are one- or two-sided
Only common tests should be described solely by name; describe more complex techniques in the Methods section.
- A description of all covariates tested
- A description of any assumptions or corrections, such as tests of normality and adjustment for multiple comparisons
- A full description of the statistical parameters including central tendency (e.g. means) or other basic estimates (e.g. regression coefficient) AND variation (e.g. standard deviation) or associated estimates of uncertainty (e.g. confidence intervals)
- For null hypothesis testing, the test statistic (e.g. F , t , r) with confidence intervals, effect sizes, degrees of freedom and P value noted
Give P values as exact values whenever suitable.
- For Bayesian analysis, information on the choice of priors and Markov chain Monte Carlo settings
- For hierarchical and complex designs, identification of the appropriate level for tests and full reporting of outcomes
- Estimates of effect sizes (e.g. Cohen's d , Pearson's r), indicating how they were calculated

Our web collection on [statistics for biologists](#) contains articles on many of the points above.

Software and code

Policy information about [availability of computer code](#)

Data collection
 Data Acquisition Software: Open Ephys (> v0.4.4, <https://github.com/open-ephys/plugin-GUI>)
 Spikesorting: Spyking Circus (> v0.8.8, <https://github.com/spyking-circus/spyking-circus>)
 Position tracking: Motive (v2.0, <https://optitrack.com/software/motive/>)

Data analysis
 Programming Language: Python 3.10
 Numpy: v1.24.4 (<https://numpy.org>)
 Scipy: v1.11.3 (<https://scipy.org>)
 Pingouin: v0.5.3 (<https://pingouin-stats.org>)
 matplotlib: v3.8.1 (<https://matplotlib.org>)
 Seaborn: v0.11.2 (<https://seaborn.pydata.org>)
 Custom general-purpose code package: NeuroPy (v0.1, <https://github.com/diba-lab/NeuroPy>)
 Custom paper-specific code package: https://github.com/diba-lab/sleep_loss_hippocampal_replay, v0.1

For manuscripts utilizing custom algorithms or software that are central to the research but not yet described in published literature, software must be made available to editors and reviewers. We strongly encourage code deposition in a community repository (e.g. GitHub). See the Nature Portfolio [guidelines for submitting code & software](#) for further information.

Data

Policy information about [availability of data](#)

All manuscripts must include a [data availability statement](#). This statement should provide the following information, where applicable:

- Accession codes, unique identifiers, or web links for publicly available datasets
- A description of any restrictions on data availability
- For clinical datasets or third party data, please ensure that the statement adheres to our [policy](#)

The processed group data for this study are available at <https://doi.org/10.7302/73hn-m920> which includes Numpy .npy files files used to generate most of the figures in this study. The remainder of the long-duration datasets generated during and analyzed for the current study will be made available by the corresponding author upon request.

Human research participants

Policy information about [studies involving human research participants and Sex and Gender in Research](#).

| | |
|-----------------------------|----------------------------------|
| Reporting on sex and gender | <input type="text" value="N/A"/> |
| Population characteristics | <input type="text" value="N/A"/> |
| Recruitment | <input type="text" value="N/A"/> |
| Ethics oversight | <input type="text" value="N/A"/> |

Note that full information on the approval of the study protocol must also be provided in the manuscript.

Field-specific reporting

Please select the one below that is the best fit for your research. If you are not sure, read the appropriate sections before making your selection.

- Life sciences Behavioural & social sciences Ecological, evolutionary & environmental sciences

For a reference copy of the document with all sections, see nature.com/documents/nr-reporting-summary-flat.pdf

Life sciences study design

All studies must disclose on these points even when the disclosure is negative.

| | |
|-----------------|--|
| Sample size | No sample size calculations were performed because we had no prior estimate of expected effect size. Based on previous experience, we surmised that a sample size of 6 animals would be sufficient to account for the potential variability in replays across animals, including an equal number of males and females. Such sample sizes were deemed reasonable based on the simultaneous recording of large numbers of units over multiple hours, with a large number of ripple events, made possible from each animal with silicon probe recordings. One of the animals had a low number of stable units, so an extra male animal was added. In 2 animals we were able to record additional sessions due to the stability of the recorded units. |
| Data exclusions | No animals were excluded from analysis. Cells that did not meet the described criterion for stability were excluded. Sessions with < 15 stable cells were excluded from reactivation and replay analyses. |
| Replication | Consistent results from individual subjects are provided in Extended Data Figures. |
| Randomization | We employed a repeated subject design, with control and sleep deprivation sessions conducted on the same animal. The order of control and sleep deprivation sessions were carried out pseudo-randomized across animals to ensure no order effects. |
| Blinding | Because sleep and awake generate distinct neuronal signatures that are easily recognized, it was not possible to maintain investigators blind to the sleep versus sleep deprivation group allocations. |

Reporting for specific materials, systems and methods

We require information from authors about some types of materials, experimental systems and methods used in many studies. Here, indicate whether each material, system or method listed is relevant to your study. If you are not sure if a list item applies to your research, read the appropriate section before selecting a response.

Materials & experimental systems

Methods

- n/a Involved in the study
- Antibodies
- Eukaryotic cell lines
- Palaeontology and archaeology
- Animals and other organisms
- Clinical data
- Dual use research of concern

- n/a Involved in the study
- ChIP-seq
- Flow cytometry
- MRI-based neuroimaging

Animals and other research organisms

Policy information about [studies involving animals](#); [ARRIVE guidelines](#) recommended for reporting animal research, and [Sex and Gender in Research](#)

- Laboratory animals
- Wild animals
- Reporting on sex
- Field-collected samples
- Ethics oversight

Note that full information on the approval of the study protocol must also be provided in the manuscript.